**The Relationship between the Summer Mesopause and Polar Mesospheric Cloud Heights**

**James M. Russell III*[a], Pingping Rong[a], Scott M. Bailey[b], Mark E. Hervig[c], and Svetlana V. Petelina[d]**

[a] Center for Atmospheric Sciences, Hampton University, Hampton, VA 23668, USA.

[b] Virginia Polytechnic Institute, Blacksburg, VA, 24061, USA.

[c] GATS, Inc., Driggs, Idaho, 83422, USA.

[d] La Trobe University, Victoria, Australia.

*Corresponding author. E-mail address: james.russell@hamptonu.edu

**Abstract**

Satellite data analyses indicate that variations of daily mean Polar Mesospheric Cloud (PMC) height and mesopause height correlate on a range of intra-seasonal time scales both short and long (i.e., ~4 days to 2 months). The average of a multiyear analysis from OSIRIS/Odin, SNOE, AIM and SABER/TIMED data sets in the polar regions north (south) of 65°N (S) show that on a daily basis the mean PMC height ($\overline{Z}_{\max}$) is located 3.5 km ± 0.5 km below the mean mesopause height ($\overline{Z}_{mes}$) in both hemispheres throughout the season and for all years examined. The data show that the relationship persists over multiple PMC seasons. This is a robust result that has also been verified with thermodynamic equilibrium and microphysical modeling. Model results from a large number of ensemble simulations show that $\overline{Z}_{\max}$ remains ~ 3.5 km below $\overline{Z}_{mes}$ as long as the vertical average of the ambient temperature minus the frost point temperature difference over the supersaturated region is about -10K or less for all the individual simulations. $\overline{Z}_{\max}$ is located less than 3.5 km below $\overline{Z}_{mes}$ for warmer supersaturated region temperatures. The

distance between the cloud and the mesopause heights ($Z_{mes} - Z_{\max}$, or $\Delta Z$) is controlled by the corresponding temperature structure in the supersaturated region. It is concluded that the variation of $\Delta Z$ is mostly driven by the variation of the temperature structure instead of the $H_2O$ mixing ratio magnitude or vertical distribution.

Key Words: Polar mesospheric clouds (PMCs); PMC height; Mesopause height; Temperature

## 1. Introduction

The polar mesospheric cloud (PMC) height is one of the fundamental variables used to describe PMC properties. PMC height has been loosely defined in several ways. For individual events observed by a variety of instruments (space-borne or ground-based) it has been defined as the altitude (tangent height for earth limb satellite measurements) where extinction, scattered limb radiance, or backscatter coefficient maximizes (sometimes referred to as $Z_{\max}$) [e.g., *Gardner et al.*, 2001; *Fiedler et. al.*, 2003; *Petelina* et al., 2006; *Hervig et al.*, 2009a]. In model simulations it is commonly referred to as the altitude where ice mass density or mean ice particle radius maximizes [e.g., *Jensen and Thomas*, 1988 (hereafter referred to as JT88); *Hervig et al.*, 2009b]. Definitions of PMC height from different perspectives basically lead to consistent results if the clouds are analyzed for highly saturated conditions such as around the summer solstice or near the peak of the cloud season about fifteen days after solstice. Uncertainties that arise either from the way PMC height is defined or from the measuring technique are factors that must be considered in interpreting results although these differences are generally small for the purposes of the study described later in this paper.

A stimulus for this current study of the relationship between mesopause and PMC heights was the occurrence of an anomalously large inter-hemispheric difference (IHD) in PMC heights in 2007 observed by the Solar Occultation For Ice Experiment (SOFIE) instrument on the AIM satellite [*Russell et al*., 2009]. SOFIE showed, for the Northern Hemisphere (NH) summer of 2007 and Southern Hemisphere (SH) summer of 2007-2008, nearly 3.5 km IHD in daily mean PMC heights (PMC are generally higher in the SH) in the beginning of the season declining to ~ 2 km at around 25 days after solstice (Figure 1). A PMC climatology using satellite data prior to 2005 [e.g. *Bailey and Merkel*, 2005; *Wrotny and Russell*, 2006] indicated only ~1.0 - 1.5 km IHD. Larger than expected IHDs, however, were observed in earlier years from ground-based lidar measurements by *Chu et al.* [2001, 2003] who reported an IHD of ~ 2-3 km. These authors suggested that the IHD in mesopause height ($Z_{mes}$ hereinafter) in 1999-2000 and 2000-2001 summers may be the cause of similar differences in the PMC height. These results prompted examination of mesopause height IHDs using six years of observations made by the Sounding of the Atmosphere using Broadband Emission Radiometry (SABER) instrument onboard TIMED satellite [*Russell et al*., 1999] and indeed, the data show an anomalously large IHD in mesopause height in 2007 driven mainly by the increased SH mesopause (Figure 2). These studies naturally led to the investigation of the relationship between the mesopause and PMC heights reported in this paper.

It is reasonable to believe that a correlation may exist between the PMC height and the mesopause height considering the fact that the vertical range of the supersaturated region needed for cloud formation varies with mesopause height. However, little has been reported concerning an actual relationship. The analysis by *Lübken et al.* [1996] using simultaneous temperature measurements from falling sphere technique and lidar detected PMCs showed no correlation between the mesopause altitude and the height of the PMC layer. On the other hand, modeling studies by JT88 indicated that the cloud peak where the largest ice particles exist is ~ 3 - 4 km below the mesopause. More recently, modeling studies using the Whole Atmosphere Community Climate Model (WACCM) with microphysics included [*Daniel Marsh*, NCAR, Private communication, 2009] and the Navy Operational Global Atmospheric Prediction System (NOGAPS) model with the Community Aerosol and Radiation Model for Atmospheres (CARMA) microphysical model included [*David Siskind*, Naval Research Laboratories, private communication, 2009;  e.g., *Rapp et al.*, 2002; Rapp and Thomas, 2006] show larger mesopause versus PMC height differences than JT88 (i.e. 5 – 7km versus 3- 4km). Based on these discrepancies, a closer look at both the PMC height itself and its relative location from the mesopause is necessary to better understand the factors that control the PMC height variation from a observation based perspective. The purpose of the current study is to examine and quantify the relationship between the two heights despite the strong intra-seasonal and inter-annual PMC variability.

Examining the PMC height and mesopause height relationship has been challenging in the past because data availability has been poor in both spatial and temporal coverage. Mesopause height has been particularly difficult to obtain since many satellite data sets either do not cover the mesosphere or their vertical resolution is too poor to precisely locate the mesopause. Lidar measurements were historically the most reliable means for determining the mesopause height and temperature [e.g., *Lübken and Müllemann*, 2003]. These measurements have the limitation that they are taken at given stations and therefore are not representative of the entire polar region. The SABER experiment on the TIMED satellite [*Russell et al.*, 1999] is one of a few satellite missions that are dedicated to middle and upper atmospheric research. The non-degrading vertical resolution of SABER (~2 km) is a particular advantage in determining the mesopause. Furthermore, the remote sensing retrieval interleave method [e.g., *Gordley et al.*, 2009; *Remsberg et al.*, 2008] used for SABER makes the identification of the mesopause even easier because the vertical spacing of the data points are ~0.4-0.5 km. At the same time, PMC data temporal and spatial coverage has increasingly improved owing to several either long-lived or recent satellite missions (e.g., Odin and AIM among others). Therefore, the time is right for examining the relationship between mesopause height and PMC height more thoroughly.

## 2. Data sets

We have used several satellite data sets in this analysis including the following: SABER/TIMED level2A v1.07 temperature in the mesosphere (see *Remsberg et al*, 2008 for validation results); OSIRIS/Odin (Optical Spectrograph and Infrared Imager System) PMC data [*Petelina et al.*, 2006, 2007]; SOFIE/AIM v1.022 $H_2O$ and PMC summary files (see *Gordley et al.*, 2009 and *Hervig et al.*, 2009a for descriptions of SOFIE retrieval and PMC detection algorithms); and SNOE (Student Nitric Oxide Explorer) PMC data [*Merkel et al.*, 2001].

SABER measures earth limb emissions in the infrared range from 1.27μm to 17μm, with kinetic temperature being retrieved from the $CO_2$ channels at 15 μm. SABER was launched in December of 2001 onboard the TIMED satellite and has been taking measurements successfully up to the current date. TIMED has an orbital inclination angle of 74.1 degree that is relatively low compared to other polar orbiting satellites, but since the satellite yaws 180° every two months SABER is able to take measurements at very high latitudes in the northern or southern hemispheres alternately with latitude coverage from 53°S-84°N or 84°S-53°N. Summer mesopause temperature and height from SABER data has been one focus of retrieval studies throughout development of different data versions and the reliability of these data has been significantly improved in the current v1.07 release [*Remsberg et al.*, 2008].

The Odin satellite was launched in February 2001 into a polar sun-synchronous and near-terminator orbit with an inclination of 97.81° [*Murtagh et al.*, 2002]. OSIRIS is one of the two instruments onboard Odin, and measures the spectra of scattered sunlight over the wavelength range 280 nm to 800 nm, with 1 nm spectral resolution. The PMC data used here is a reprocessed version provided by *Petelina et al.* [2006, 2007] who processed enhanced scattered limb radiance profiles taken in the polar summer mesospheric mode to detect PMC events. OSIRIS PMC brightness is available in two forms; relative brightness as a ratio of the measured radiance at PMC peak to the corresponding Rayleigh background or absolute brightness in units of $10^{10}$ photons $sr^{-1}$ $cm^{-2}$ $nm^{-1}$ $sec^{-1}$. In the current data version absolute brightness at 291 nm is used. A well known issue of the limb viewing geometry is that the clouds detected could be at the tangential altitude or in the far/near-field. In this regard the "true" position is always in question with the consequence that the actual cloud altitude could be higher than what is determined. Although a lower boundary of, say, 80 km, can be set to exclude the unrealistically low clouds, the cloud heights that appear quite normal could still come from the PMCs that are actually higher. This problem is less significant when the PMCs are strong and exhibit distinct centroid heights [private communication, *Jörg Gumbel*, Stockholm University, Sweden], such as, in the peak of the season around the summer solstice. OSIRIS provides an excellent data source to study the correlation between mesopause and PMCs in the extended polar cap region because it was launched around the same time as SABER and has near-global data coverage (82°S to 82°N).

SOFIE is a solar occultation instrument onboard the AIM satellite launched in April of 2007 that measures temperature, water vapor, and other trace gases in the mesosphere in addition to its primary mission of monitoring PMCs. SOFIE latitude coverage is from 65° to 84° north and south. Extinction profiles are measured in eight wavelength bands ranging from 0.330 µm to 5.006 µm. Water vapor is retrieved from channel 3 at 2.462 µm and 2.618 µm, and PMC properties are from channel 5 at 3.064 µm and 3.186 µm, respectively. SOFIE limb observations also have the same far/near-field issue with PMC height determination as discussed for OSIRIS.

SNOE is an earlier mission that also measured PMCs (1998-2003) [*Merkel et al*., 2001; *Bailey et al*., 2005]. Two seasons of SNOE data (2003 north and south) are available before it was turned off to serve as a check on OSIRIS/SABER findings. SNOE is an ultra violet spectrometer that measures limb scattered sunlight by nitric oxide (NO) at 215.0 nm and 236.5 nm. Although observed NO scattering occurred mainly above 95 km altitude, scattering at higher altitudes produces NO effects in the lower altitude retrieval. These contributions were removed from the radiances by the SNOE team prior to the PMC retrieval. After removal of the NO contribution, the radiance includes Rayleigh scattering by nitrogen and oxygen molecules and backward and forward Mie scattering by PMCs. PMCs were detected from both SNOE channels. PMC brightness in the SNOE retrievals refers to the ratio of PMC brightness to an average Rayleigh background at 83 km (i.e., scattering ratio). North and south PMC brightnesses can be biased relative to each other by 30 times or more due to the smaller scattering angle in the south (<90°) versus the north (>90°). In the following analysis we have excluded all the SNOE clouds for which the brightness is greater than 50 and this only occurs in the SH. The threshold of 50 was chosen because 99% of the observed clouds have a SR of 50 or less. The 1% with larger SRs are anomalously bright. Further their peak altitudes are anomalously high and their inclusion would significantly lift the mean cloud height. The SNOE team has determined that these anomalously bright and high clouds are the result of high levels of NO during that time period that are not being fully accounted for in the algorithms. The team has verified that these clouds should not be included in the present analysis [*Bailey et al.*, 2005].

## 3. Observations

### 3.1 The relationship between the daily mean mesopause height and PMC height

Figure 3 shows the intra-seasonal variation of the daily mean PMC height and mesopause height minus 3.5 km, for both hemispheres and for years 2002, and 2005-2007. Mesopause heights are obtained from analyzing SABER temperature profiles, and PMC heights are from SNOE and OSIRIS PMC data. A polar regional average is performed for both variables using all the measurements north/south of 65°N/S. The time series does not go beyond 25 days after the solstice because TIMED satellite yaws at this time and SABER polar coverage ends. The daily mean PMC height is calculated using the formula $\bar{Z}_{\max} = \sum Z_{\max\_i} \cdot Brgt_{\max\_i} \big/ \sum Brgt_{\max\_i}$ , where $Z_{\max}$ is the PMC height, $i$ is the index of the PMC events, and $Brgt_{max}$ is the cloud brightness at $Z_{\max}$. The PMC heights are weighted by the brightness to focus this study on the most intense clouds and to make the daily mean PMC heights measured by different instruments comparable without the necessity of setting up thresholds for cloud brightness to account for differing instrument sensitivities.

We note from Figure 3 that $\bar{Z}_{\max}$ and the daily mean mesopause height ($\bar{Z}_{mes}$) minus 3.5 km present very similar intra-seasonal variations, and furthermore their values show fairly close agreement throughout the time period. Wavelet analysis (not shown) has revealed that in some cases the agreement exists on a range of periods from a few days to seasonal scales. However deviation from the 3.5 km difference does exist for a significant number of days. For example, in some instances in both hemispheres in the earlier part of the season the deviation is notable with the clouds being at lower altitudes than the 3.5 km difference would predict. One possible reason for this to occur is that the mesopause in the early season is systematically higher than the OSIRIS cloud detection algorithm cutoff at 88 km [*Petelina et al,* 2006; *Petelina et al.*, 2007].

In order to test whether 3.5 km is a significant number, the daily mean mesopause – PMC height difference, i.e., $\overline{Z}_{mes} - \overline{Z}_{\max}$, or $\Delta\overline{Z}$ hereinafter, for NH, SH, and both hemispheres combined are examined statistically in Figure 4, using all the daily means shown in Figure 3. Binned by 0.5 km, all three distributions show peaks at the bin centered at 3.5 km. The data points that fall into the three bins centered at 3.5 km±0.5 km take up ~86% of all daily mean values.

Figure 5 shows a similar plot as Figure 3 except for using SOFIE mesopause height and PMC height in the 2007 NH and 2008 NH, respectively. In this case ice mass density is used rather than brightness because it is directly retrieved from SOFIE observations. Only the NH case is shown because the SOFIE v1.022 SH mesopause height has a known negative bias relative to other datasets (e.g., SABER and ACE) that is currently being investigated. The SOFIE mesopause height and PMC height relationship shows a qualitatively similar characteristic to what is shown in the SABER/OSIRIS/SNOE analysis, but only for the time period ~5 - 10 days before the summer solstice to ~ 40 days after. Earlier or later in the season, SOFIE PMCs occur at notably higher altitudes than the $\Delta\overline{Z}$ = 3.5 km would predict.

The degree of agreement between the SABER mesopause minus 3.5 km and the OSIRIS/SNOE PMC height is sufficient to suggest a potential underlying mechanism that connects the two heights, given its zero statistical mean and relatively small degree of spread (Figure 4). On the other hand, the vacillation around the $\Delta\overline{Z}$ = 3.5 km is equally important and worthy of clarification. Also, understanding the SOFIE NH mesopause and PMC height relationship is vital in providing a wider perspective on this subject. Model studies were conducted to interpret these findings and results are discussed in Section 4 in this paper.

**3.2 Lack of latitudinal dependence in the polar summer region (>65°N/S)**

We have so far discussed a previously unreported observation of a relationship between the polar summer mesopause and PMC heights, i.e., $\Delta\overline{Z}$ = 3.5 km. Note that we have performed the analysis assuming that the latitudinal dependence of PMC and mesopause heights is not significant. In order to verify that latitude is unimportant in the calculations shown thus far, we examined the latitude dependence of $Z_{mes}$ and $Z_{max}$.

Figure 6 shows a latitude versus days from solstice (DFS) cross section of the zonal mean SABER mesopause height in the 2007 northern and southern summers respectively. For both hemispheres, latitude ranges north/south of 65°N/S are shown. The southern hemisphere case is a shorter time series because SABER data are not available in January 2008. SABER ascending and descending nodes, corresponding to approximately two daily local times, do not make any qualitative difference in the results (not shown), indicating that the mesopause height is not sensitive to the local time. We can see significant intra-seasonal variability in both panels but it shows no consistent latitudinal gradient. This means that on a daily basis the polar regional average can accurately represent the features of entire polar region. Analysis of SABER data for different years (not shown) indicates qualitatively the same features, i.e., north/south of 65°N/S in the polar summer, the mesopause height zonal daily mean is not latitude dependent. But it should be noted that the range of latitude considered is important in making this argument since the above conclusions may not be true for lower latitudes (50°-65°N/S) where PMCs are also observed. PMCs detected in the 50°-60°N/S range by lidar for example, were at lower altitudes than those detected at high polar latitudes [*Chu et al.,* 2004]. In the 50°-60°N/S range the

SABER mesopause height also has its lowest global values (not shown), and for some years this low mesopause is slightly extended into the 65°-70°N/S range.

Figure 7 shows the intra-seasonal variation of the 2007 OSIRIS daily mean PMC height, cloud brightness, and the number of detected clouds, for latitude bands with 5-degree increments and for the entire region, respectively. For OSIRIS on the daily basis the geometric average of $Z_{max}$ is slightly lower than the brightness weighted average. Although qualitatively negligible, this difference indicates a considerable number of dim clouds at low $Z_{max}$ in the OSIRIS record. Figures 7a-7b indicate very small latitudinal variations in $Z_{max}$ in both hemispheres, with the exception that the most equatorward clouds (at 65-70°N/S) can be slightly lower on occasion. In latitude range 65°-70°N/S the number of PMC events is smaller and the clouds are dimmer, and both variables tend to increase towards higher latitudes. The lower cloud heights for the 65°-70°N/S range could be a demonstration of the latitude dependence of the PMC height at the lowest latitudes as discussed above, but due to the smaller number of clouds the statistics are less reliable. Also, the centroid altitudes of relatively dim clouds are more difficult to determine, and there is a real possibility that these dimmer clouds were in the near- or far-field of the limb view.

The lack of latitudinal dependence in the PMC height is further supported by the SNOE PMC data in 2002-2003 (Figure 8). SNOE is a spinning satellite with a normal spin period of ~12 seconds. This speed is 6-10 times faster than one OSIRIS scan. SNOE data points in one orbit are oversampled (~0.75° latitude increment for each spin), resulting in much denser data coverage in one orbit than for OSIRIS. A characteristic of SNOE PMCs is that the SH PMCs are nearly an order of magnitude brighter than the NH counterparts primarily because of the drastically different scattering angles in the two hemispheres [*Merkel et al.*, 2001; *Bailey et al.*, 2005]. Since the cloud brightness (i.e., scattering ratio for SNOE) is used in calculating the daily mean PMC height, this hemispheric difference has to be carefully considered. We found that some extraordinarily bright clouds (>100.0) in the SH lead to significant differences between the geometric mean and the brightness weighted mean. We resolved this issue by excluding some very bright clouds (~1%) using an upper brightness limit of 50. We found that increasing this limit to as much as 70 does not affect the result. Under this condition the weighted and unweighted daily mean PMC heights are nearly identical in both hemispheres. Due to a considerably larger number of measurements from SNOE, excluding some events does not degrade the reliability of the daily mean values. Figure 8 upper panels show that the daily mean PMC heights for the different latitudinal bands are nearly identical, and that this is true for both hemispheres. The lack of latitudinal dependence in $Z_{max}$ is more pronounced in SNOE than in the OSIRIS results. The seemingly lower PMC height in the 65°-70°N/S range shown in OSIRIS is not seen in SNOE.

## 4. Model simulations of the PMC height

### 4.1 0-D model description and rationale in the current study

A zero-dimensional PMC model (referred to as 0-D model hereinafter) was developed by *Hervig* et al.[2009b] to simulate PMC ice mass density ($M_{ice}$) versus altitude assuming that ice exists in thermodynamic equilibrium (i.e. no microphysics is involved in the model simulations). They considered saturation vapor pressures over ice from either *Mauersberger and Krankowsky* [2003] (MK03) or *Murphy and Koop* [2005] (MK05), and found that using MK03 generally yielded greater $M_{ice}$ and ice at higher temperatures. The 0-D approach neglects the time dependence of ice growth, sedimentation, horizontal and vertical transport, and sublimation. It is labeled as 0-D because the equilibrium state is directly reached without experiencing any development stage. The 0-D model results resemble the asymptotic state of a more complex micro-physics model such as CARMA (*Turco* et al., 1982; *Jensen et al.*, 1989; *Jensen and Thomas*, 1994; *Rapp and Thomas*, 2006). Given the initial temperature, pressure and water vapor, CARMA reaches a near-steady state within less than 24 hours, which somewhat justifies the approach of using either the asymptotic state of CARMA or the 0-D modeled state to simulate the daily mean state of the PMCs.

*Hervig et al.* [2009b] presented modeled PMC ice mass density vs. altitude using SOFIE temperature and $H_2O$ profiles. When using the MK05 vapor pressures, the model results were able to reproduce the observed $Z_{max}$ to within -0.1 km, and the observed mass density at $Z_{max}$ to within 16%.

The 0-D model simulates the ice mass density using the environmental temperature, water vapor, and air pressure, and because it is computationally inexpensive it is ideal for simulating PMC conditions for large ensembles of observations. In this work 0-D simulations were conducted for SABER temperature profiles and SOFIE temperature and water vapor profiles in 2007. The model uses one pair of co-located and simultaneous measurements of temperature and $H_2O$ profiles to generate one PMC event and assumes a direct association between the PMCs and their local thermodynamic surroundings. This could at first sight contradict some of the previous studies. For example, simultaneous temperature and PMC measurements using the lidar technique did not show any direct correlation between the mesopause height and PMC height [*Lübken et al.*, 1996]. *Hansen* and *von Zahn* [1994] also argued that there is only a limited dependence between the NLC/PMC displays and their local thermal conditions; instead, the conditions along the particle trajectory must be taken into account. Modeling studies [e.g., *von Zahn* and *Berger*, 2003; *Berger* and *von Zahn*, 2007] were conducted in several later papers to investigate the ice particle trajectories, depicting a hypothetical picture of one particle undergoing significant vertical and latitudinal excursions within 24 hours. Wave analysis conducted by *Merkel et al.* [2009] using SABER temperature and CIPS/AIM (Cloud Imaging and Particle Size) PMC data [*Rusch et al.*, 2008] suggested that a significant phase shift exists between the coldest temperature and the brightest cloud. It is so far inconclusive as to whether it is the PMC waves, the PMC transport, temperature waves or some combination of these factors that makes the short term (<1 day) variability so complex.

The primary use and advantage of the 0-D model lies in its ability to obtain an ensemble mean (i.e., daily, polar regional mean) state of the PMCs without involving any complicated advection or vertical transport processes that create the short term (< 1 day) and spatial variability. Each simulation using one pair of temperature and $H_2O$ profiles (i.e., from SABER or SOFIE) is taken as being representative of the daily PMC behavior. The very good agreement between the 0-D model results calculated in this paper and the observations indicate that spatial and temporal details (<1 day) of the PMCs, which are not well known, do not change their mean state in any substantial way.

### 4.2 Input conditions

To acquire an overall understanding of all the input conditions that will be used we present in Figure 9 the mesopause temperature for all events in the NH from SABER and SOFIE, and the SOFIE water vapor vertical profiles throughout the season together with a reference water vapor profile taken from *Rapp and Thomas* [2006]. The pressure is taken from SABER data or SOFIE data depending on which data set is being used. Figure 9a shows the 2007 NH mesopause temperature for all SABER measurements in a latitude range centered at the SOFIE latitudes ±0.5 degree, along with all SOFIE measured mesopause temperatures throughout the season. It shows that there are some very low mesopause temperatures (<130 K) present in

SABER but not in SOFIE. This is not unexpected because SOFIE temperatures in the vicinity of the mesopause appear to have a warm bias and current efforts are underway to better understand this situation. However, the majority of SABER temperatures (large gray dots) are above 130K, which supports the argument that at SOFIE latitudes the temperatures are generally warmer than 130K. Comparisons of NH SOFIE and SABER temperature profiles in most of the mesosphere show excellent agreement (<3K) for a coincidence box of 2° in latitude, 10° in longitude, and 2 h in time (see Figure 10). In Figure 9b, the SABER temperatures shown in the 9a are repeated, and the remaining SABER events north of 65°N are shown by the small black dots. Although polar summer mesospheric temperature is generally colder at higher latitudes, the two subsets indicate that cold and warm events are not strictly separated by latitude ranges. Apparently there are some very cold SABER temperatures at SOFIE latitudes. Although fewer in number, these low temperatures could support some fairly strong PMCs at lower latitudes, depending on the water vapor availability. The water vapor volume mixing ratio (vmr) profiles used as input are shown in Figure 9c including the reference water vapor used in *Rapp and Thomas* [2006] and the SOFIE daily mean profiles throughout the 2007 summer season. SABER temperature profiles for any given day are paired up with either the reference $H_2O$ or the daily mean SOFIE $H_2O$ profile of the same day to perform the 0-D model simulations. The MK05 saturation vapor pressure formulation was chosen in this study. The use of MK05 or MK03 saturation vapor pressure has a finite impact on the ice top and ice bottom altitudes, i.e., the MK05 scheme causes ~0.5 km higher cloud height values than the MK03 scheme.

### 4.3 0-D model results

#### 4.3.1 Intra-seasonal variation of the daily means

The modeled intra-seasonal variation of the daily mean $Z_{max}$ and $Z_{mes}$ - 3.5 km are shown in Figure 11a using SABER temperatures with the reference $H_2O$ (Figure 9c), and in Figure 11b using SABER temperatures with the SOFIE daily mean $H_2O$ profile. One SABER event produces one cloud if the temperature ($T$) is less than the frost point temperature ($T_f$ hereinafter) in the vicinity of the mesopause. The daily mean mesopause height ($\overline{Z}_{mes}$) is calculated using only those events that generated the clouds. Ice mass density weighting is applied when calculating $\overline{Z}_{\max}$. We have sorted the SABER events by the mesopause temperature prior to the model simulation. Figures 11c-11d show $\overline{Z}_{\max}$ and $\overline{Z}_{mes}$-3.5 km obtained from using a subset of the profiles with the top 10 coldest mesopause temperature (coldest-10). We note from Figure 11 that the intra-seasonal variations of $\overline{Z}_{\max}$ and $\overline{Z}_{mes}$ show close agreement and the values of $\overline{Z}_{\max}$ and $\overline{Z}_{mes}$-3.5 km agree very well with only small deviations. SOFIE daily mean $H_2O$, which increases (i.e., by ~3-4 ppmv) as the season progresses, causes slightly lower cloud altitudes (~0.2-0.5 km) on some days, but the overall impact is small. A sensitivity study conducted by *Lübken et al.* [2007] using the CARMA model indicated that multiplying a given water vapor profile by a factor of 10 will lead to ~2 km decrease of the PMC peak height, which suggests that it takes a drastic $H_2O$ change to yield a moderate change in the cloud height. It is therefore reasonable to conclude that in the real atmosphere water vapor plays only a minor role in the cloud height variation.

As for the deviations from $\Delta\overline{Z}$ = 3.5 km, a most obvious feature is that in the coldest-10 case, $\overline{Z}_{\max}$ tends to be lower than the $\overline{Z}_{mes}$- 3.5 km while in the all-event case it is the opposite. This consistent difference between the two cases suggests that colder mesopause temperatures are linked to, on average, lower cloud heights. The possible temperature control is further supported by a similar set of model simulations shown in Figure 12 that used observed SOFIE temperature and $H_2O$ profiles. All SOFIE events with the mesopause temperature below the frost point (obtained from the corresponding $H_2O$ profiles) are used to conduct the 0-D simulations. We note in Figure 12 the same features as seen in SOFIE observations in Figure 5, i.e., around summer solstice and ~ 40 days later the 3.5 km difference is better held but in the earlier and later season the clouds are higher. The separation between $\overline{Z}_{\max}$ and $\overline{Z}_{mes}$-3.5 km, however, is larger than in the observations. One reason for this is that $\overline{Z}_{mes}$-3.5 km in Figure 12 appears at a lower altitude than in Figure 5 especially for solstice and later times and more so for 2008 than 2007. This is because SOFIE observed mesopause heights are lower for those temperature profiles that met the condition of $T - T_f < 0$. What also contributes to the larger separation is the fact that in the earlier or later season $\overline{Z}_{\max}$ is higher than what is shown in Figure 5. The suspected warm bias in SOFIE temperature can probably account for most of this.

#### 4.3.2 Dependence of PMC height on $T - T_f$ averaged over the supersaturated region

Figure 13 shows 2007 NH and SH scatter plots of individual simulations on the plane of a height index vs. a temperature index. All the simulations using the SABER temperatures are included regardless of the day of the season. The temperature index is defined as the vertical average of the ambient temperature minus the frost point temperature, i.e., $\left\langle T - T_f \right\rangle$, where the angular brackets represent the average over the altitude range where supersaturation exists. The height index is $3.5km - \Delta Z$, where $\Delta Z = Z_{mes} - Z_{\max}$, so that falling on the zero line indicates precisely 3.5 km difference. A striking feature in Figure 13a is that in the cold temperature range (i.e., $\left\langle T - T_f \right\rangle$ < -10K) the points are scattered above and below the 3.5 km line with comparable fractions, while $\Delta Z$ decreases steadily at warmer temperatures. Both ice mass density weighted and geometric means of $\Delta Z$ are computed for each 1.0K bin, shown by the large symbols. The weighted version shows ~ 0.1-0.2 km lower cloud height but both the weighted and unweighted profiles are close to the 3.5 km difference line in the cold temperature range. The weighted mean cloud heights are slightly lower because in the model simulation the lower clouds have greater mass density. Figure 13b shows the SH case which indicates cloud height distributions that are fairly consistent with the NH case. This suggests that the mesopause and PMC height relationship remains the same even if the clouds are formed at a significantly higher altitude and lower ambient air pressure, as is the case for 2007 SH. Another noteworthy point is that using reference $H_2O$ or SOFIE daily mean $H_2O$ makes only slight differences in the cloud heights, demonstrated by the near-perfect overlap between the dark and light gray dots and a ~0.1-0.3 km difference in the mean cloud heights averaged over the temperature bins.

The variability of the modeled PMC heights above and below the “3.5 km” line stems from the variability in the model input conditions. In a similar scatter plot shown in Figure 14, the vertical axis is replaced by 3.5km– ($Z_{mes}$ –$Z_{S=1}$), where $Z_{S=1}$ is the lower altitude point of $S=1$ and S represents the saturation ratio. $Z_{S=1}$ can be used as another characteristic height because NLCs exist between $Z_{mes}$ and $Z_{S=1}$[e.g., *Höffner et al.*, 2003]. The distribution of the points in Figure 14 is nearly identical to what Figure 13 has shown except that they are shifted downward systematically by ~ 0.5 to 1.0 km. The ~ 0.5 to1.0 km difference is simply a result of the 0-D model mechanism showing that the largest water vapor mass density in excess of saturation assigned to the ice phase occurs ~ 0.5-1.0 km above the lower bound of supersaturated region. This distance is generally supported by observations although it was interpreted from a different viewpoint in previous studies. For example JT88 considered this difference to be a result of the balancing effect between the sedimentation and sublimation. The strong resemblance between

Figures 13 and 14 suggests that the structure ($Z_{mes}$-$Z_{S=1}$) and the strength ($\langle T - T_f \rangle$) of the supersaturated region fully determines the PMC height in a 0-D model simulation.

#### 4.3.3 Variability of the modeled PMC height for any given $\langle T - T_f \rangle$

The relationship between $\Delta\overline{Z}$ and $\langle T - T_f \rangle$ is definite but the individual simulations have shown a range of $\Delta Z$ values for a given $\langle T - T_f \rangle$, mainly because of the variability in $Z_{max}$. The vertical profiles of $T$, $T_f$, and ice mass density for a few selected simulations under conditions of (a) cold temperatures ($\langle T - T_f \rangle$ = -15 K) with $\Delta Z$ being < 3.5 km, equal to 3.5 km, and >3.5 km; and (b) warm temperature ($\langle T - T_f \rangle$ = -3 K) with $\Delta Z$ being <3.5 km, and >3.5 km, are shown in Figure 15.

Under cold condition (a) the three mesopause temperatures or heights in Figure 15a are very similar to each other but their lower vertical bounds for the supersaturated region ($Z_{S=1}$) show large differences. The profiles that present a more downward extended supersaturated region tend to have lower cloud peaks. Under cold temperatures these three types of occurrences appear with nearly equal probability between the mesopause and the PMC heights, resulting in a mean difference of ~3.5 km. Under warm condition (b) when the temperature is marginally below the frost point, results show that in the majority of cases (see dashed curve in Figure 15b), the cloud will form just in the vicinity of mesopause without much flexibility to grow at any lower altitudes. The significant decrease of $\Delta\overline{Z}$ (or increase of 3.5 km-$\Delta\overline{Z}$) for the warmer temperatures in Figure 13 is a reflection of the narrowing distance between the two heights. In a rare but possible case (solid curve in Figure 15b), which did occur in some of our simulations, there is a broad temperature structure that is uniformly separated from the corresponding $T_f$ line by less than 5 K. Due to the larger water vapor abundance at lower altitudes a strong ice peak occurs at a relatively low altitude, that is 5.4 km below the mesopause in this particular simulation. Figures 13 and 15 together indicate that the mean difference of 3.5 km or less between the mesopause and PMC heights is a statistical outcome that is governed by the temperature in the vicinity of the mesopause.

**4.4 1-D CARMA model simulations of the PMC heights**

Theoretically speaking, nucleation, sedimentation of the ice particles, and the vertical wind, are essential processes in a PMC model to better represent the cloud formation and variation. We, however, have just shown that a model with all these processes ignored has successfully reproduced the observed PMC and mesopause height relationship. Questions necessarily arise regarding the roles of these processes in the PMC height determination. We have used the CARMA model [*Rapp and Thomas*, 2006] to briefly investigate these issues. We have chosen the simplest CARMA 1-D scenario assuming spherical particles and meteoric smoke with a uniform vertical distribution as ice nuclei. The CARMA default vertical wind profile was used, which imposes a persistent upwelling with a maximum speed of ~ 4.2 cm/s at around 86 km. The radiative transfer and gravity wave drag are turned off. Different model schemes were detailed in a CARMA review paper by *Rapp and Thomas* [2006]. In the current study, the model output occurs at the end of a 24-hour simulation, and the simulations were performed using individual SABER events together with the reference $H_2O$ profile (see Figure 9b-9c). Figure 16a shows a scatter plot using all the CARMA simulations. A similar distribution to that obtained using the 0-D model occurs, but a few significant differences do exist.

The primary difference between CARMA and the 0-D model results is that the mean cloud height from CARMA is about 1.0-1.5 km lower in the cold temperature range ($\langle T - T_f \rangle$ < -

10 K). It was found that at the end of a 24-hour period the ice peak mass density is about twice as large as the 0-D model result, and the mean ice particle radius at the cloud peak reaches 80-100 nm regularly. It appears that the fall velocity applied to these large particles has led to a strongly intensified and narrowed ice mass density peak at a systematically lower altitude. In this case, the mean PMC heights are significantly closer to the bottom of the supersaturated region. Increasing the vertical wind speed was considered as a possible remedy. A sensitivity study has shown however, that an increase of the upwelling rate (~2.0-3.0 cm/s originally) by a factor of up to 5.0, which is already unrealistic, is unable to lift the cloud height because it will result in longer exposure of the ice particles to the prevailing environment and cause further growth of ice. A more efficient approach to reduce the low bias in the CARMA modeled cloud height is to decrease the ice particle growth rate so that the sedimentation is significantly weakened. All the simulations shown in Figure 16a are repeated using a growth rate that is one-third of the default value but with all the remaining conditions unchanged. A similar scatter plot (Figure 16b) indicates that the mean cloud heights in the cold temperature range are significantly lifted (by ~0.5-0.7 km) and show closer agreement with the 0-D model result.

In the warm temperature range for $\langle T - T_f \rangle$ > -6K, CARMA simulations using the default growth rate show a large separation between the weighted mean and the geometric mean cloud height (plus and diamond symbols). In fact the weighted version of $\Delta\overline{Z}$ shown in Figure 16a remains at ~ 3.5 km in the warm temperature range. This characteristic suggests that the PMC height is dominated by a few strong clouds while the majority of clouds are too weak to contribute much to the weighted mean PMC height. The extreme brightness variation between the strong and weak clouds is attributed to the ice particle growth microphysics. The Kelvin effect (i.e. the effect of particle size on saturation vapor pressure) strongly limits the growth of the small ice particles; but as long as the barrier is exceeded, the growth will be overly fast using the model default growth rate. In the case with the changed growth rate (Figure 16b) the separation becomes less severe, showing qualitative agreement with the 0-D model result.

The CARMA model study indicates that although the nucleation and vertical transport are indispensible elements of a model to faithfully reproduce the PMC evolution, several uncertainties arise from including these processes. The better agreement between the 0-D model results and observations suggests that the mean cloud peak altitude mostly remains at the altitude where water vapor mass density in excess of saturation is the largest. Vertical transport plays only a minor role in adjusting the curve upwards or downward.

## 5. Summary

The relationship between the PMC height and the mesopause height has been examined in the polar summer region using both satellite data analysis and modeling studies. The intra-seasonal variations of the mesopause height and the PMC height averaged daily over the polar region (north/south of 65°N/S) agree over a range of time scales from 4-5 days to seasonal scales. Analysis of SNOE/OSIRIS/SABER PMC and mesopause heights for 2002 and 2005-2007, shows that on average there is a ~3.5 km distance between the mesopause height and the PMC height in both hemispheres throughout the season with ~ 86% of the $\Delta\overline{Z}$ values falling in the range of 3.5±0.5 km. SOFIE 2007-2008 NH mesopause height and PMC height show the same relationship on days around summer solstice and ~ 40 days after, but in the earlier or later season the PMC peak altitudes are systematically closer to the mesopause than a 3.5 km distance would predict.

A 0-D PMC model was used to interpret the mesopause and PMC height relationship on a daily mean basis. A large number of simulations were performed using SABER and SOFIE measurements in 2007 (temperature and $H_2O$) as input conditions at polar latitudes. Model results indicate that the vertical average of the temperature difference from the frost point temperature ($\langle T - T_f \rangle$) in the supersaturated region determines the ensemble mean of the mesopause minus PMC height difference, i.e., if $\langle T - T_f \rangle$ < -10 K, the mean difference is ~3.5 km, while if $\langle T - T_f \rangle$ > -10K, the difference is less than 3.5 km. The PMC height in the latter case is closer to the mesopause height. For individual model simulations $Z_{mes} - Z_{max}$ falls above or below the line of the "3.5 km difference", depending on the vertical structure of $T$ - $T_f$ in the supersaturated region. Examination of $H_2O$ profile effects shows that the $H_2O$ mixing ratio is of minor importance in affecting the mesopause and PMC height relationship.

**Acknowledgements**. This work was supported under NASA contract NAS5-03132. Many thanks are given to the AIM and SOFIE team for support, valuable discussion, and advice. Thanks also to the SABER/TIMED retrieval team for providing SABER level 2A data. We are very grateful to the OSIRIS/Odin and SNOE PMC data retrieval and development teams. We are also grateful to the individual scientists who had developed CARMA model to its current stage, in particular Michael Stevens who had made our access of CARMA model possible in a timely manner and meanwhile provided valuable help. Odin is currently a third party mission for the European Space Agency.

**References**

Bailey, S.M., A.W. Merkel, G.E. Thomas, and J.N. Carstens (2005), Observations of polar mesospheric clouds by the Student Nitric Oxide Explorer, *J. Geophys. Res.*, *110*, D13203, doi:10.1029/2004JD005422.

Berger, U, and U. von Zahn (2007), Three-dimensional modeling of the trajectories of visible NLC particles indicates that these particles nucleate well below the mesopause, *J. Geophys. Res.*, *112*, D16024, doi:10.1029/2006JD008106.

Chu, X., C. S. Gardner, and G. Papen (2001), Lidar observations of polar mesospheric clouds at South Pole: Seasonal variations, *Geophys. Res. Lett.*, 28, 1203–1206.

Chu, X., C.S. Gardner, R.G. Roble (2003), Lidar studies of interannual, seasonal, and diurnal variations of polar mesospheric clouds at the South Pole, *J. Geophys. Res.*, *108*(D8), 8447, doi:10.1029/2002JD002524.

Chu, X., G. J. Nott, P. J. Espy, C. S. Gardner, J. C. Diettrich, M. A. Clilverd, and M. J. Jarvis (2004), Lidar observations of polar mesospheric clouds at Rothera, Antarctica (67.5°S, 68.0°W), *Geophys, Res. Lett.*, *31*, doi:10.1029/2003GL018638.

Gardner, C.S., G. C. Papen, X. Chu, and W. Pan (2001), First lidar observations of middle atmosphere temperatures, Fe densities, and polar mesospheric clouds over the North and South Poles, *Geophys. Res. Lett.*, *28(7)*, 1199-1202.

Gordley L.L., M. E. Hervig, C. Fish, J. M. Russell III, S. Bailey, J. Cook, S. Hansen, A. Shumway, G. Paxton, L. Deaver, B. T. Marshall, J. Burton, B. Magill, C. Brown, E. Thompson, J. Kemp (2009), The solar occultation for ice experiment, *J. Atmos. Sol.-Terr. Phys.*, *71*, doi:10.1016/j.jastp.2008.07.012.

Fiedler, J., G. Baumgarten and G. von Cossart (2003), Noctilucent clouds above ALOMAR between 1997 and 2001: Occurrence and Properties, *J. Geophys. Res., 108 (D8),* 8453, doi:10.1029/2002JD002419.

Hansen, G., U. von Zahn(1994), Simultaneous observations of noctilucent clouds and mesopause temperatures by lidar, *J. Geophys. Res.*, *99*(D9), 18, 989-18, 999.

Hervig, M.E., L.L. Gordley, M. Stevens, J.M. Russell, S. Bailey, and G. Baumgarten (2009a), Interpretation of SOFIE PMC measurements: Cloud identification and derivation of mass density, particle shape, and particle size, *J. Atmos. Solar-Terr. Phys.*, *71*, doi:10.1016/j.jastp.2008.07.009.

Hervig, M. E., M. H. Stevens, L. L. Gordley, L. E. Deaver, J. M. Russell, and S. Bailey (2009b), Relationships between PMCs, temperature and water vapor from SOFIE observations, *J. Geophys. Res.*, *114*, D20203, doi:10.1029/2009JD012302,.

Höffner, J., C. Fricke-Begemann, and F. –J. Lübken (2003), First observations of noctilucent clouds by lidar at Svalbard, 78°N, *Atmos. Chem. Phys.*, *3*, 1101-1111.

Jensen, E., and G. E. Thomas (1988), A Growth-Sedimentation Model of Polar Mesospheric Clouds' Comparison with SME Measurements, *J. Geophys. Res.*, *93*(D3), 2461-2473.

Jensen, E., G.E. Thomas, O.B. Toon (1989), On the diurnal variation of noctilucent clouds, *J. Geophys. Res.*, *94*, 14 693–14 702.

Jensen, E., G.E. Thomas (1994), Numerical simulations of the effects of gravity waves on noctilucent clouds, *J. Geophys. Res.*, *99*, 3421–3430.

Lübken, F-J., K.-H Fricke and M. Langer (1996), Noctilucent clouds and the thermal structure near the Arctic mesopause in summer, *J. Geophys. Res.*, *101*(D5), 9489 – 9508.

Lübken, F-J., and A. Müllemann (2003), First in situ temperature measurements in the summer mesosphere at very high latitudes (78°N), *J. Geophys. Res.*, *108*, doi: 10.1029/2002JD002414.

Lübken, F-J., M. Rapp, and I. Strelnikova (2007), The sensitivity of mesospheric ice layers to atmospheric background temperatures and water vapor, *Advances in Space Research*, *40*, 794-801, doi:10.1016/j.asr.2007.01.014.

Mauersberger, K., and D. Krankowsky (2003), Vapor pressure above ice at temperatures below 170 K, *Geophys. Res. Letters*, *30*, doi:10.1029/2002GL016183.

Merkel, A.W., and C. A. Barth (2001), Altitude determination of ultraviolet measurements made by the Student Nitric Oxide Explorer, *J. Geophys. Res.*, *106*(A12), 30,283-30,290.

Merkel, A. W., D. W. Rusch, S. E. Palo, J. M. Russell III, S. M. Bailey (2009), Mesospheric planetary wave effects on global PMC variability inferred from AIM-CIPS and TIMED/SABER for the northern summer 2007 PMC season, *J. Atmos. Sol-Terr. Phys.*, *71*, doi:10.1016/j.jastp.2008.12.001

Murphy, D. M., and T. Koop, Review of the vapour pressure of ice and super- cooled water for atmospheric applications(2005), *Quart. J. R. Met. Soc.*, *131*, 1539-1565.

Murtagh, D.P., et al.(2002), An overview of the Odin Atmospheric Mission, *Can. J. Phys*, *85*, 309–319.

Petelina, S., E. J. Llewellyn, D. A. Degenstein, N. D. Lloyd (2006), Odin/OSIRIS limb observations of polar mesospheric clouds in 2001–2003, *J. Atmos. Sol-Terr. Phys.*, *68*, doi:10.1016/j.jastp.2005.08.004.

Petelina, S., E. J. Llewellyn, D. A. Degenstein (2007), Properties of polar mesospheric clouds measured by ODIN/OSIRIS in the northern hemisphere in 2002-2005, *Can. J. Phys.*, *85*, 1143-1158, doi:10.1139/P07-092.

Rapp, M., F.-J. Lübken, A. Müllemann, G.E. Thomas, E.J. Jensen (2002), Small scale temperature variations in the vicinity of NLC: experimental and model results. *J. Geophys. Res.*, *107* (D19), 4392, doi:10.1029/2001JD001241.

Rapp, M., G.E. Thomas (2006), Modeling the microphysics of mesospheric ice particles: assessment of current capabilities and basic sensitivities. *J. Atmos. Sol-Terr. Phys.*, *68*, 715–744.

Remsberg, E. E., B. T. Marshall, M. Garcia-Comas, D. Krueger, G. S. Lingenfelser, J. Martin-Torres, M. G. Mlynczak, J. M. Russell III, A. K. Smith, Y. Zhao, C. Brown, L. L. Gordley, M. J. Lopez-Gonzalez, M. Lopez-Puertas, C.Y. She, M. J. Taylor, and R. E. Thompson (2008), Assessment of the quality of the Version 1.07 temperature versus pressure profiles of the middle atmosphere from TIMED/SABER, *J. Geophys. Res.*, *113*, D17101, doi:10.1029/2008JD010013.

Rusch, D.W., G. E. Thomas, W. McClintock, A. W. Merkel, S. M. Bailey, J. M. Russell III, C. E. Randall, C. Jeppesen, and M. Callan (2008), The Cloud Imaging and Particle Size Experiment on the Aeronomy of Ice in the Mesosphere Mission: Cloud Morphology for the Northern 2007 season, *J. Atmos. Sol.-Terr. Phys.*, *71*, doi:10.1016/j.jastp.2008.11.005 .

Russell III, J. M., M.G. Mlynczak, L.L. Gordley, Larry , J. J. Tansock, and R. Esplin (1999), Overview of the SABER experiment and preliminary calibration results, *Proc. SPIE Vol. 3756*, 277-288, *Optical Spectroscopic Techniques and Instrumentation for Atmospheric and Space Research III, Oct.*.

Russell III, J. M., S. M. Bailey, L. L.Gordley, D. W. Rusch, M. Hora´nyi, M. E.Hervig, G. E. Thomas, C. E. Randall, D. E. Siskind, M. H. Stevens, M. E. Summers, M. J. Taylor, C. R. Englert , P. J. Espy, W. E. McClintock, A. W. Merkel (2009), The Aeronomy of Ice in the Mesosphere (AIM) mission: Overview and early science results, *J. Atmos. Sol-Terr. Phys.*, *71*, doi:10.1016/j.jastp.2008.08.011.

Turco, R.P., O.B. Toon, R.C. Whitten, R.G. Keesee, and D. Hollenbach (1982), Noctilucent clouds: simulation studies of their genesis, properties and global influences, *Planetary and Space Science, 30*, 1147–1181.

Wrotny, J. E., and J. M. Russell III(2006), Inter-hemispheric differences in polar mesospheric clouds observed by the HALOE instrument, *J. Atmos. Sol-Terr. Phys.*, *68*, doi:10.1016/j.jastp.2006.05.014.

von Zahn, U., and U. Berger (2003), Persistent ice cloud in the midsummer upper mesosphere at high latitudes: Three dimensional modeling and cloud interactions with ambient water vapor, *J. Geophys. Res.*, *108*(D8), 8451, doi:10.1029/2002JD002409.

**Figure captions**

**Figure 1:** Summer intra-seasonal variations of v1.022b SOFIE measured PMC height in 2007 for both hemispheres and the hemispheric differences. The thin and thick lines are daily mean and the 8-day smoothed time series, respectively. The PMC heights are weighted by the corresponding peak mass densities. The vertical bars indicate Standard Error of the Mean (SEM) levels for the daily mean time series, but they are shown only at the 8-day smoothed data points. The half-length of the bar is the root-mean-square of the SEMs for the eight data points centered at the large symbols.

**Figure 2:** Summer intra-seasonal variations of the SABER daily mean mesopause height for both hemispheres and their hemispheric differences. Daily mean values are calculated using temperature profiles north/south of 65°N/S.

**Figure 3:** Summer intra-seasonal variations of SABER mesopause height minus 3.5 km and the PMC height from SNOE and OSIRIS. Both mesopause height and PMC height are daily mean values north/south of 65°N/S, and the PMC heights are weighted by the corresponding peak cloud brightness values. The vertical bars represent the Standard Error of the Mean.

**Figure 4:** Number of days on which the daily mean mesopause height minus PMC height fall into different ranges of values. The bin width is 0.5 km. All data in the previous figure are included.

**Figure 5:** Northern summer intra-seasonal variations of SOFIE mesopause and PMC heights in 2007 and 2008. Daily means are calculated using all the profiles in the summer

hemisphere, and the daily PMC height is weighted by the ice mass density at the cloud peak. As in Figure 3 the SEM bars are also shown but only on one side for clear presentation.

**Figure 6:** Latitude versus time cross section of SABER mesopause height (km) in 2007 polar summer regions. The latitude bins are 2.5 degree each and all events within the bins daily are used to calculate the daily averages. The interval between adjacent contours is 0.5 km.

**Figure 7:** Summer intra-seasonal variations of OSIRIS variables for different latitude bands in the 2007 NH (left) and SH (right). Both the daily mean (thin) and 8-day smoothed daily mean (thick with symbols) are shown. (Upper) Brightness weighted PMC height, (middle) number of PMC detected, and (lower) PMC brightness ($10^{10}$ photons $sr^{-1}$ $cm^{-2}$ $nm^{-1}$ $sec^{-1}$).

**Figure 8:** Similar to Figure 7 except for SNOE PMC analysis.

**Figure 9:** Input and initial conditions used in the model studies. (a) SOFIE and SABER mesopause temperatures (black and gray) in comparable latitude ranges. Daily SABER profiles are chosen for the SOFIE latitude +/- 0.5 degree. Panel (b) repeats the gray dots in the left panel and shows all the remaining SABER mesopause temperatures north of 65°N with small black dots. (c) A reference $H_2O$ profile (thick dash line) and a series of SOFIE daily mean $H_2O$ profiles in the 2007 NH summer (solid lines). The different shades of color represent a sequence of days of year as the numbers indicated on the right.

**Figure 10:** Comparison of SOFIE and SABER NH temperature profiles in June and July, 2007-2008. The comparison is based on 359 pairs of coincidences selected using the criteria of 10° in longitude, 2° in latitude, and 2 h in time.

**Figure 11:** Intra-seasonal variations of 0-D modeled daily mean PMC heights weighted by the cloud peak ice mass density and the corresponding daily mean SABER mesopause heights. (Upper) Model results using all SABER temperature profiles north of 65°N, and (lower) using SABER profiles with the top 10 coldest mesopause temperatures. (Left) model results using the reference $H_2O$ profile, and (right) using SOFIE daily mean $H_2O$ profiles.

**Figure 12:** Similar to Figure 11 except for the modeling results using all SOFIE temperature and $H_2O$ profiles.

**Figure 13:** Scatter plots of the individual 0-D simulations using SABER temperature profiles north/south of 65°N/S for all days combined, and for (a) 2007 NH, and (b) 2007 SH. The vertical axis is 3.5 km-$\Delta Z$, so that the zero line indicates precisely 3.5 km difference between the two heights. The horizontal axis is the temperature difference from the frost point averaged over the supersaturated region. The dark and pale gray colors are for reference $H_2O$ and SOFIE daily mean $H_2O$, respectively. The large symbols are the mean values of the small dots in each 1 K bin (see legends), and both geometric mean and the ice mass density weighted mean are calculated.

**Figure 14:** Similar to Figure 13 except that the cloud height is replaced by the lower altitude limit of the supersaturated region. The mean PMC heights (large plus and dot signs)

in Figure 13 are repeated to reveal the distance of the 0-D modeled PMC height and the lower altitude limit of the supersaturated region.

**Figure 15:** Examples of individual 0-D simulations using a few selected SABER temperature profiles and the reference $H_2O$ profile. (Left) Cold temperature case, when temperature difference from the frost point is around -15K. The angular brackets represent the vertical average defined in Figure 13. (Right) Warm temperature case, when the temperature difference is around -3 K. The squares are for peak locations, and the numbers next to them are values of 3.5 km-ΔZ, if negative the PMC peak is more than 3.5 km from the mesopause.

**Figure 16:** Scatter plots of CARMA individual simulations using all SABER temperature profiles north of 65°N in 2007 NH. Only reference $H_2O$ is used. Vertical axis and the horizontal axis are the same as in Figure 13. The two panels are for simulations using different ice growth rates, (a) default ice growth rate in CARMA, and (b) a changed growth rate by factor of 0.33 from the default value.

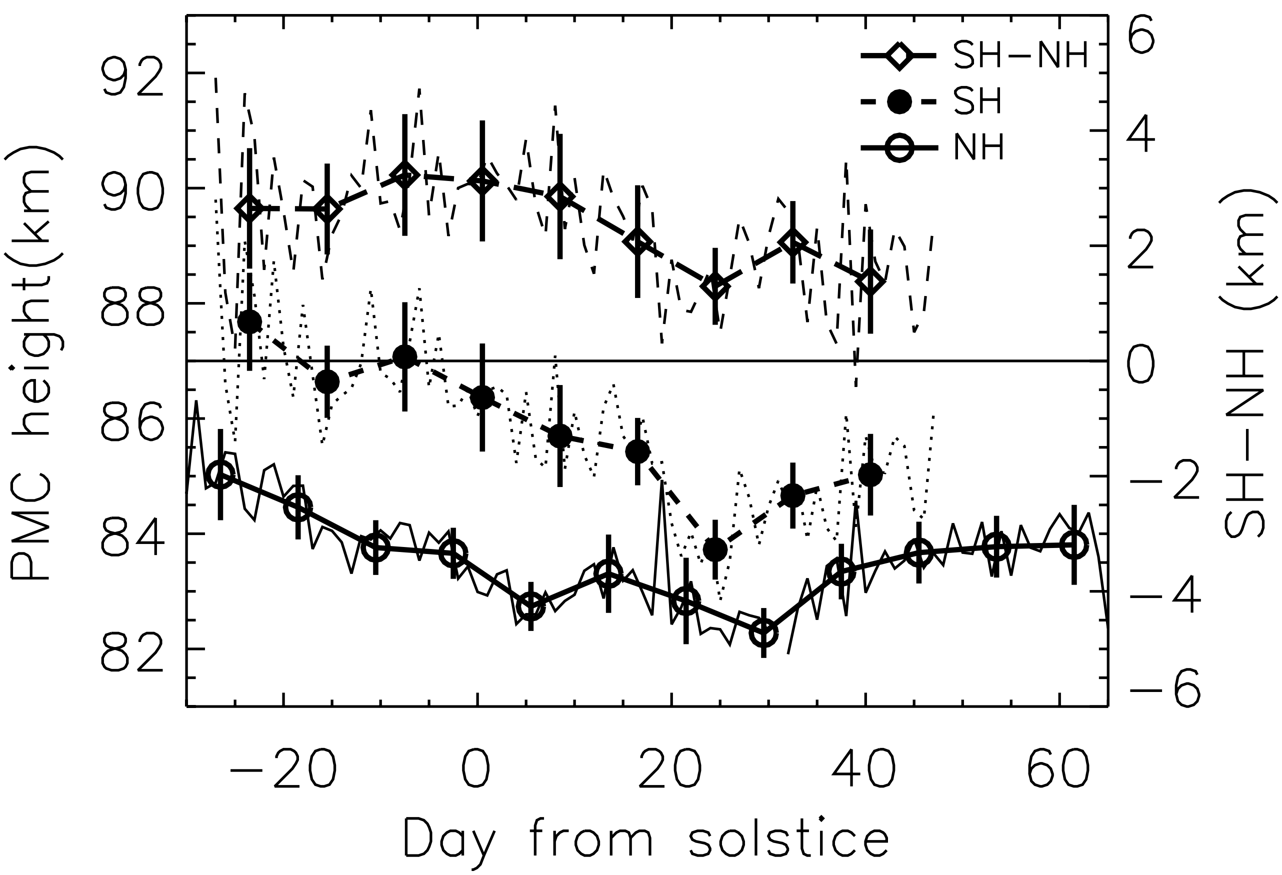
SH−NH
SH
NH
PMC height(km)
SH−NH (km)
Day from solstice
92
90
88
86
84
82
6
4
2
0
−2
−4
−6
−20
0
20
40
60

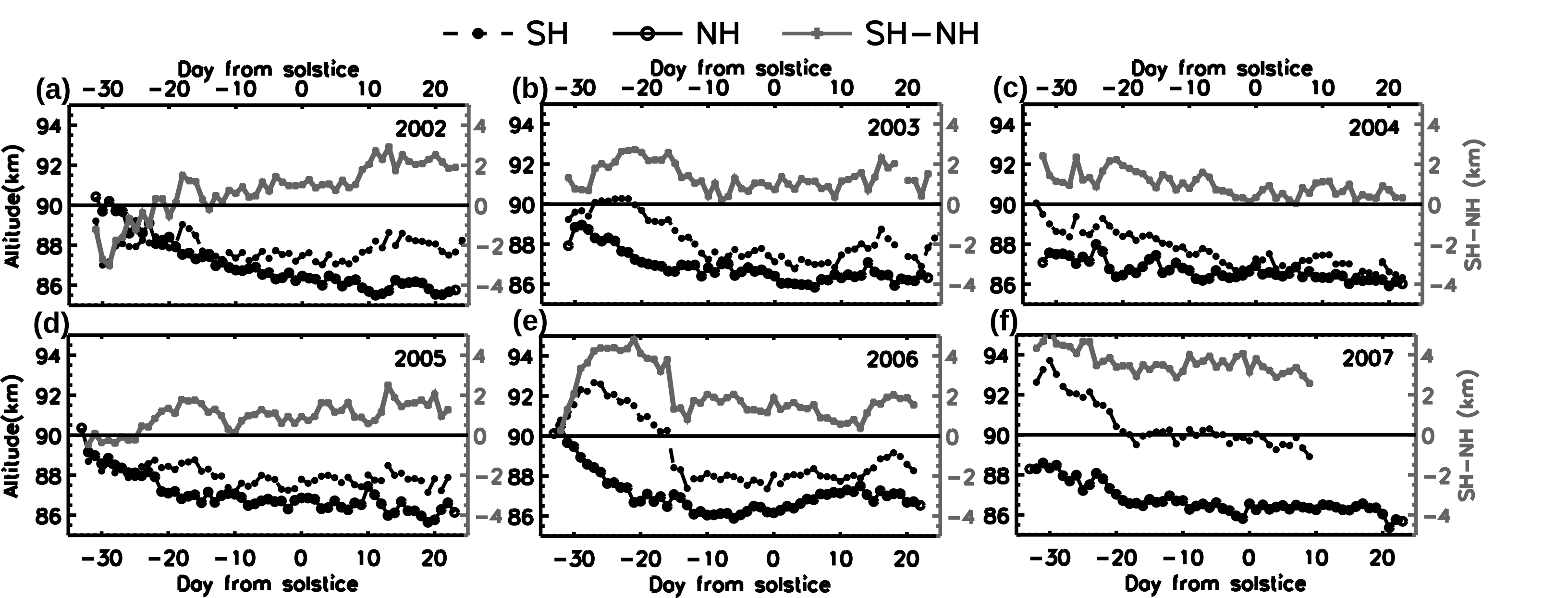
SH
NH
SH−NH
Day from solstice
(a)
2002
(b)
2003
(c)
2004
(d)
2005
(e)
2006
(f)
2007
Altitude(km)
SH−NH (km)

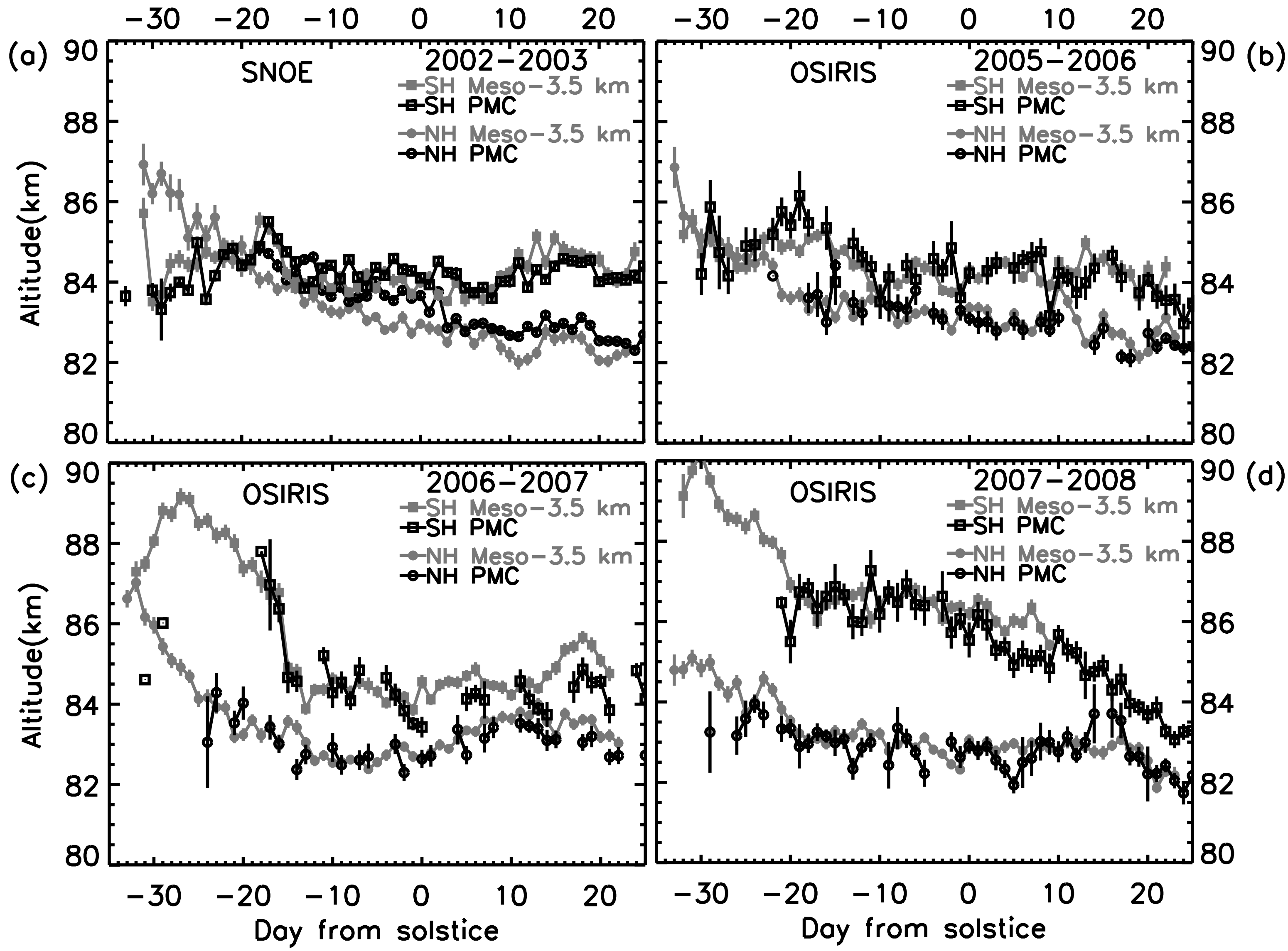

(a)
SNOE
2002–2003
SH Meso−3.5 km
SH PMC
NH Meso−3.5 km
NH PMC
(b)
OSIRIS
2005–2006
SH Meso−3.5 km
SH PMC
NH Meso−3.5 km
NH PMC
(c)
OSIRIS
2006–2007
SH Meso−3.5 km
SH PMC
NH Meso−3.5 km
NH PMC
(d)
OSIRIS
2007–2008
SH Meso−3.5 km
SH PMC
NH Meso−3.5 km
NH PMC
Altitude(km)
Day from solstice

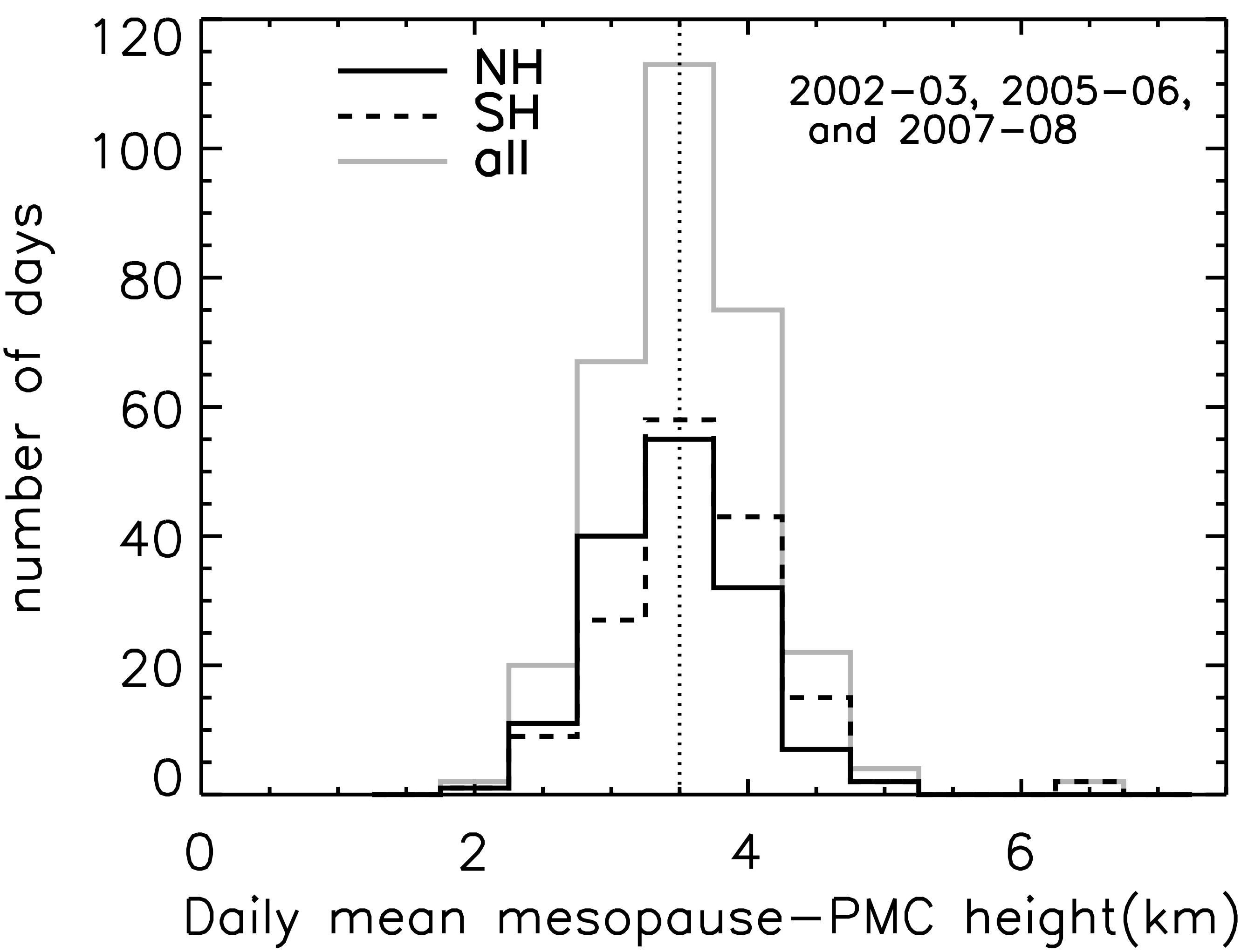

NH
SH
all
2002-03, 2005-06, and 2007-08
number of days
Daily mean mesopause-PMC height(km)
0
20
40
60
80
100
120
0
2
4
6

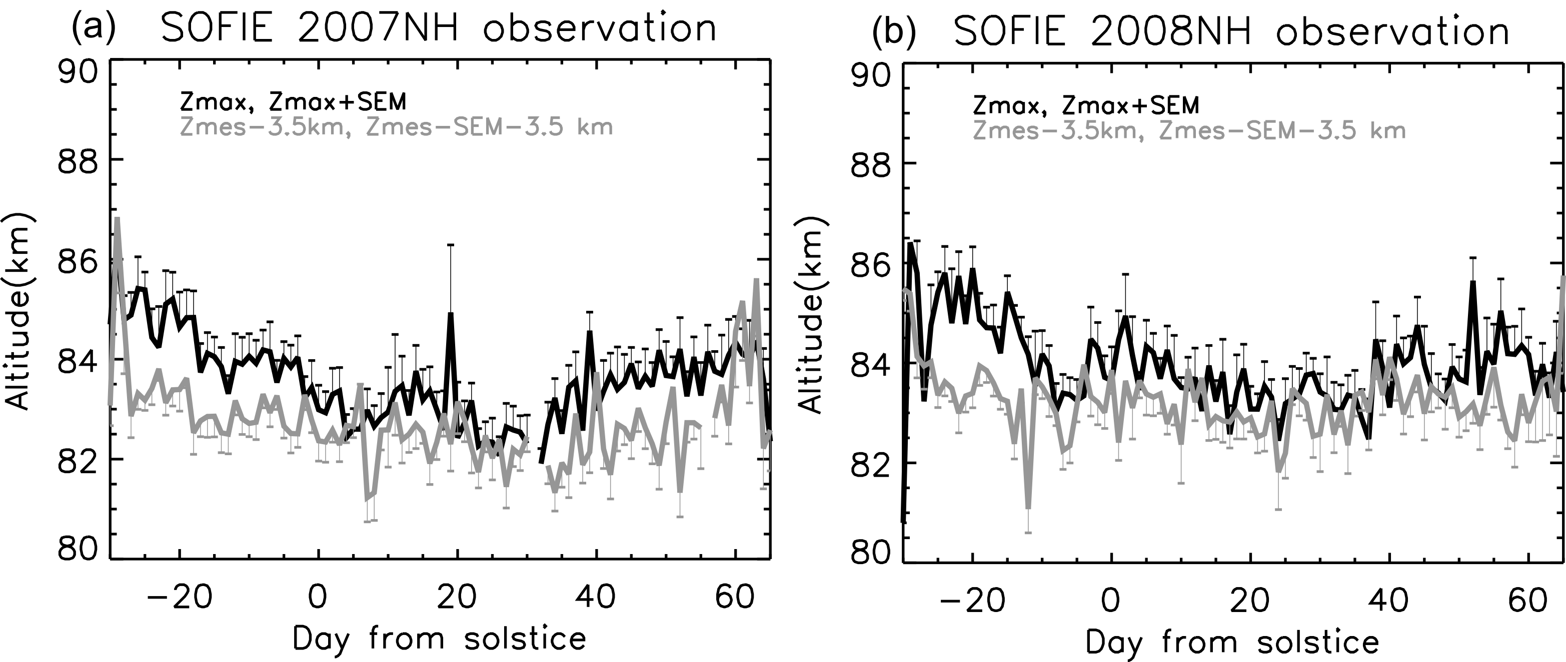

(a) SOFIE 2007NH observation
Zmax, Zmax+SEM
Zmes−3.5km, Zmes−SEM−3.5 km
Altitude(km)
Day from solstice
(b) SOFIE 2008NH observation
Zmax, Zmax+SEM
Zmes−3.5km, Zmes−SEM−3.5 km
Altitude(km)
Day from solstice

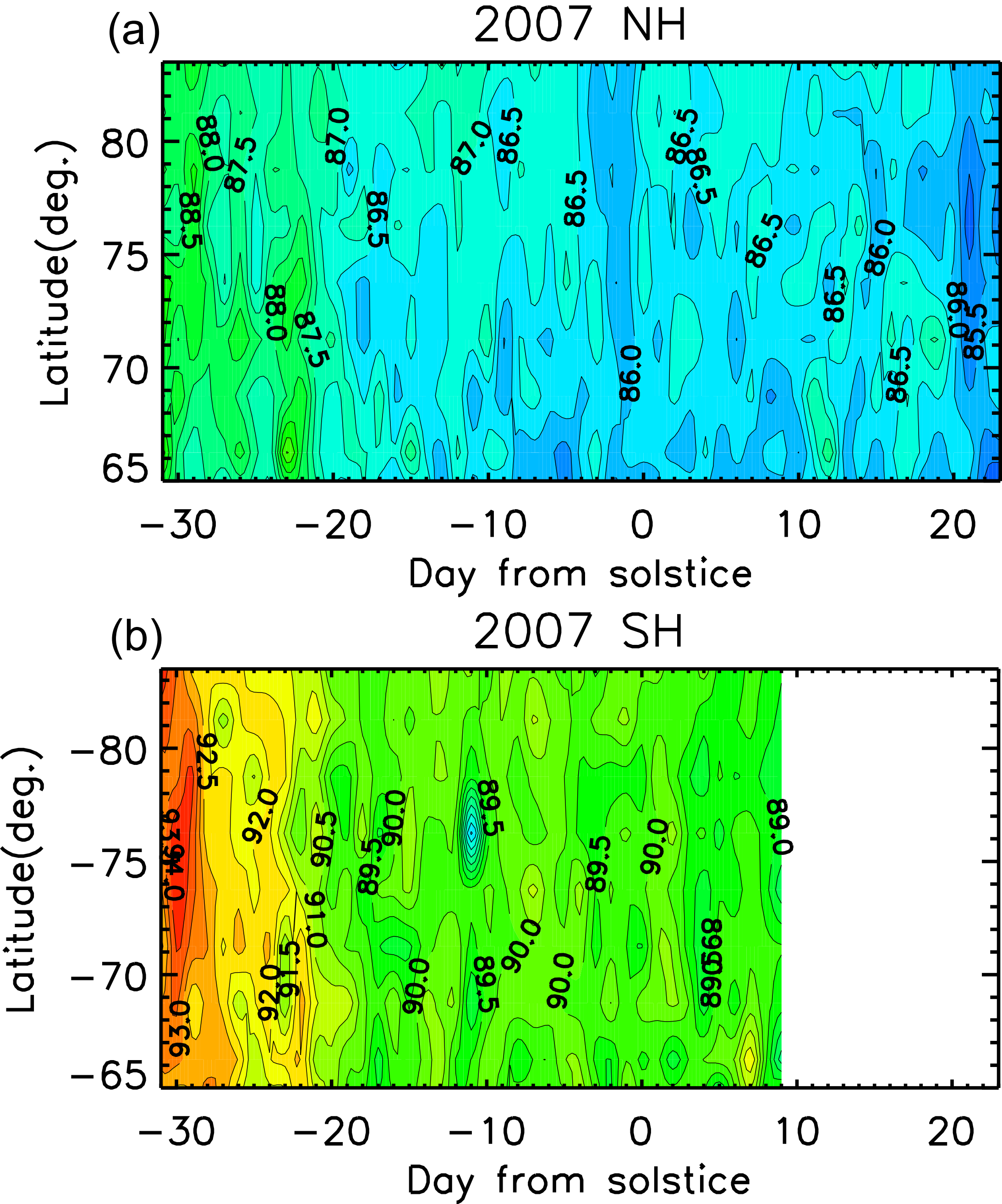
(a)
2007 NH
Latitude(deg.)
80
75
70
65
−30
−20
−10
0
10
20
Day from solstice
(b)
2007 SH
Latitude(deg.)
−80
−75
−70
−65
−30
−20
−10
0
10
20
Day from solstice

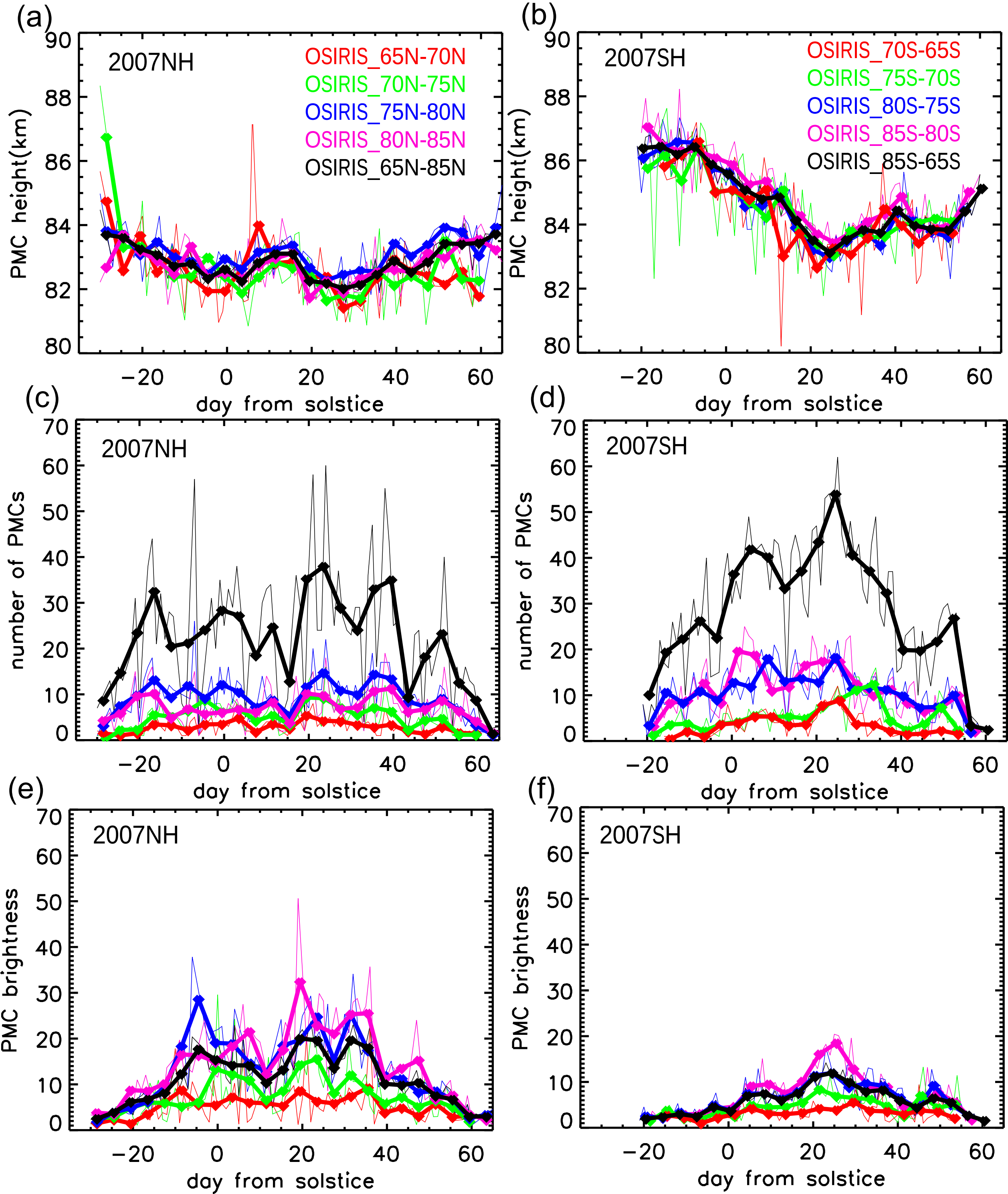

(a)
2007NH
OSIRIS_65N-70N
OSIRIS_70N-75N
OSIRIS_75N-80N
OSIRIS_80N-85N
OSIRIS_65N-85N
PMC height(km)
day from solstice
(b)
2007SH
OSIRIS_70S-65S
OSIRIS_75S-70S
OSIRIS_80S-75S
OSIRIS_85S-80S
OSIRIS_85S-65S
PMC height(km)
day from solstice
(c)
2007NH
number of PMCs
day from solstice
(d)
2007SH
number of PMCs
day from solstice
(e)
2007NH
PMC brightness
day from solstice
(f)
2007SH
PMC brightness
day from solstice

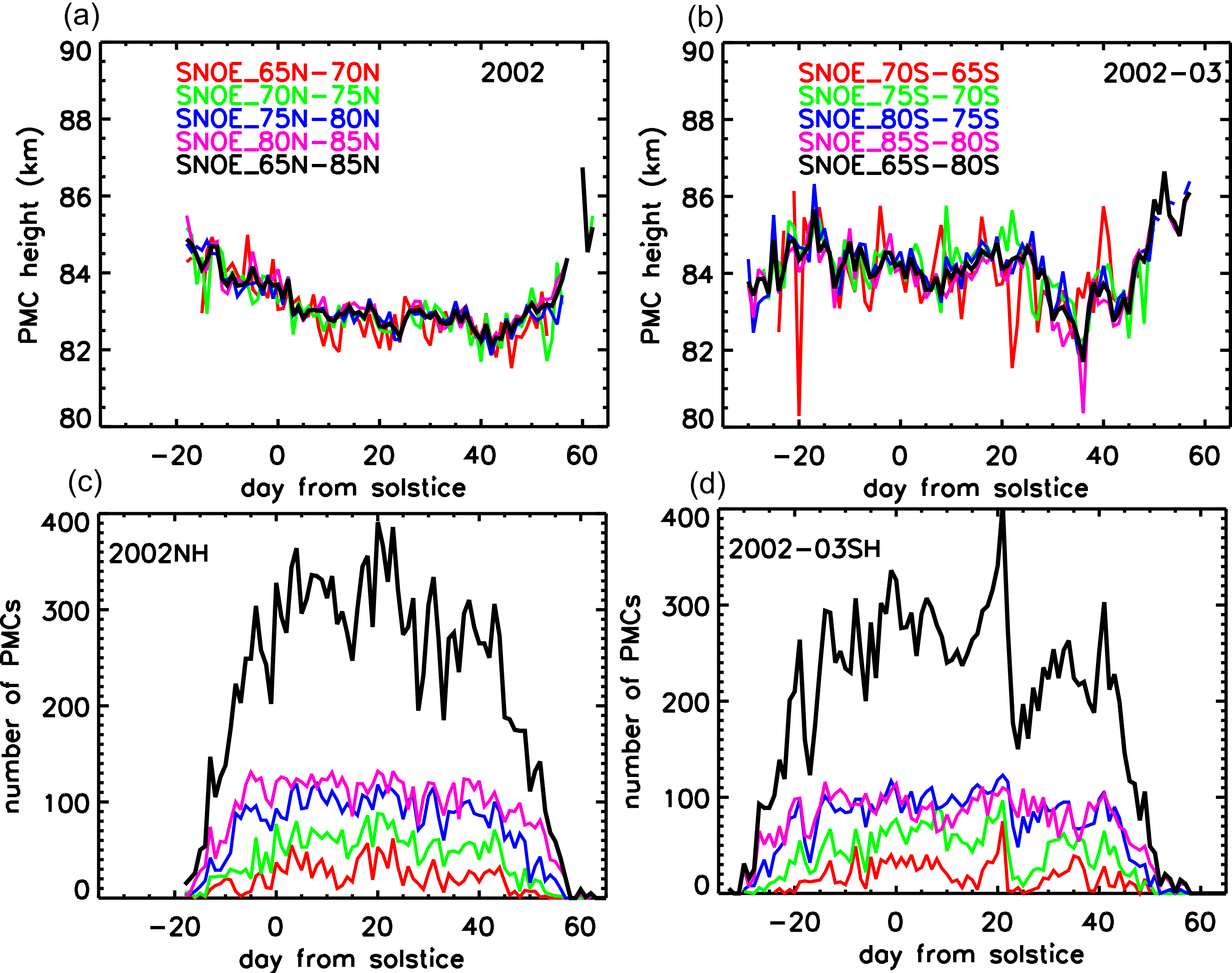

(a)
SNOE_65N-70N
SNOE_70N-75N
SNOE_75N-80N
SNOE_80N-85N
SNOE_65N-85N
2002
PMC height (km)
day from solstice
(b)
SNOE_70S-65S
SNOE_75S-70S
SNOE_80S-75S
SNOE_85S-80S
SNOE_65S-80S
2002-03
PMC height (km)
day from solstice
(c)
2002NH
number of PMCs
day from solstice
(d)
2002-03SH
number of PMCs
day from solstice

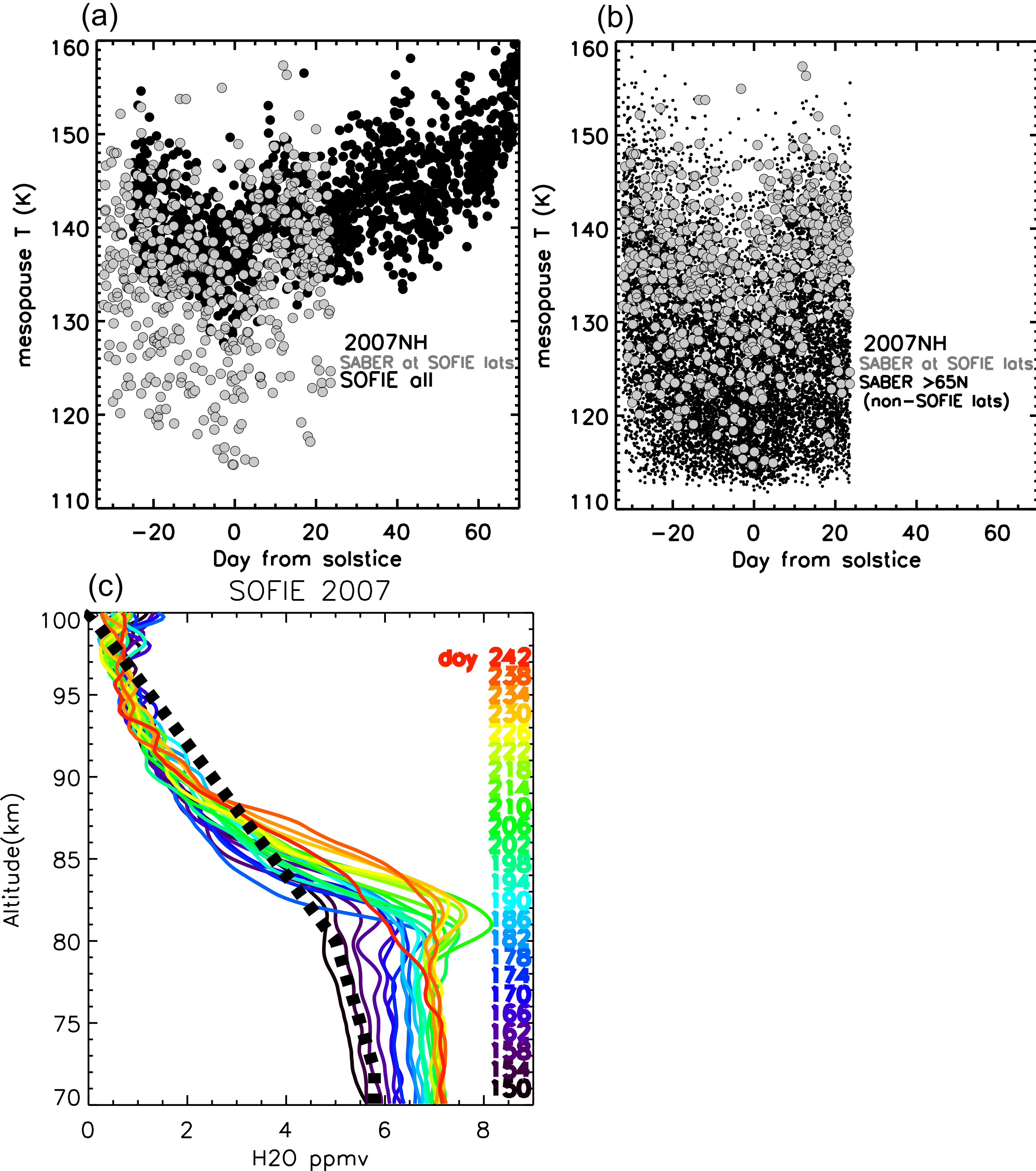
(a)
mesopause T (K)
Day from solstice
2007NH
SABER at SOFIE lats
SOFIE all
(b)
2007NH
SABER at SOFIE lats
SABER >65N
(non-SOFIE lats)
(c)
SOFIE 2007
Altitude(km)
H2O ppmv
day 242
238
234
230
226
222
218
214
210
206
202
198
194
190
186
182
178
174
170
166
162
158
154
150

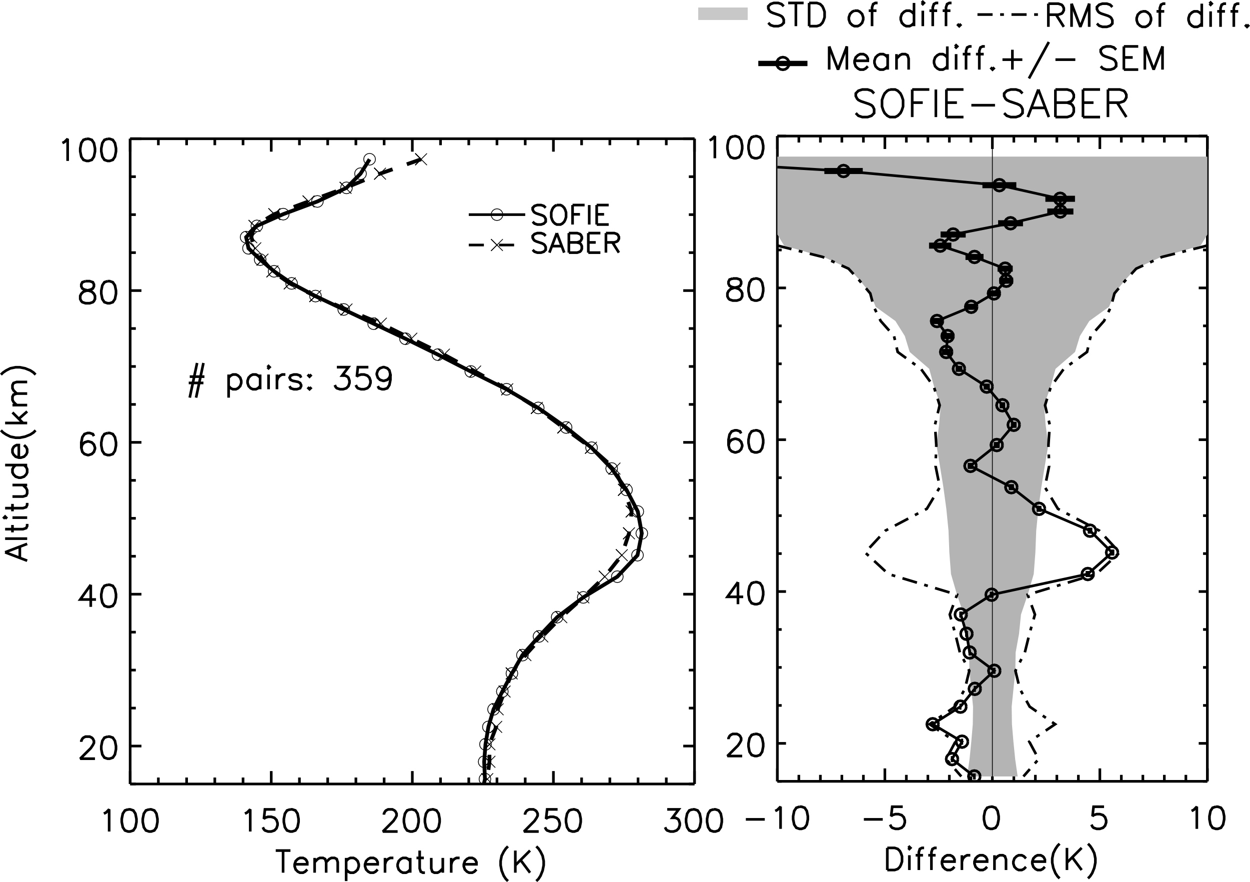
STD of diff.
RMS of diff.
Mean diff.+/- SEM
SOFIE-SABER
SOFIE
SABER
# pairs: 359
Altitude(km)
Temperature (K)
Difference(K)
100
80
60
40
20
100
150
200
250
300
-10
-5
0
5
10

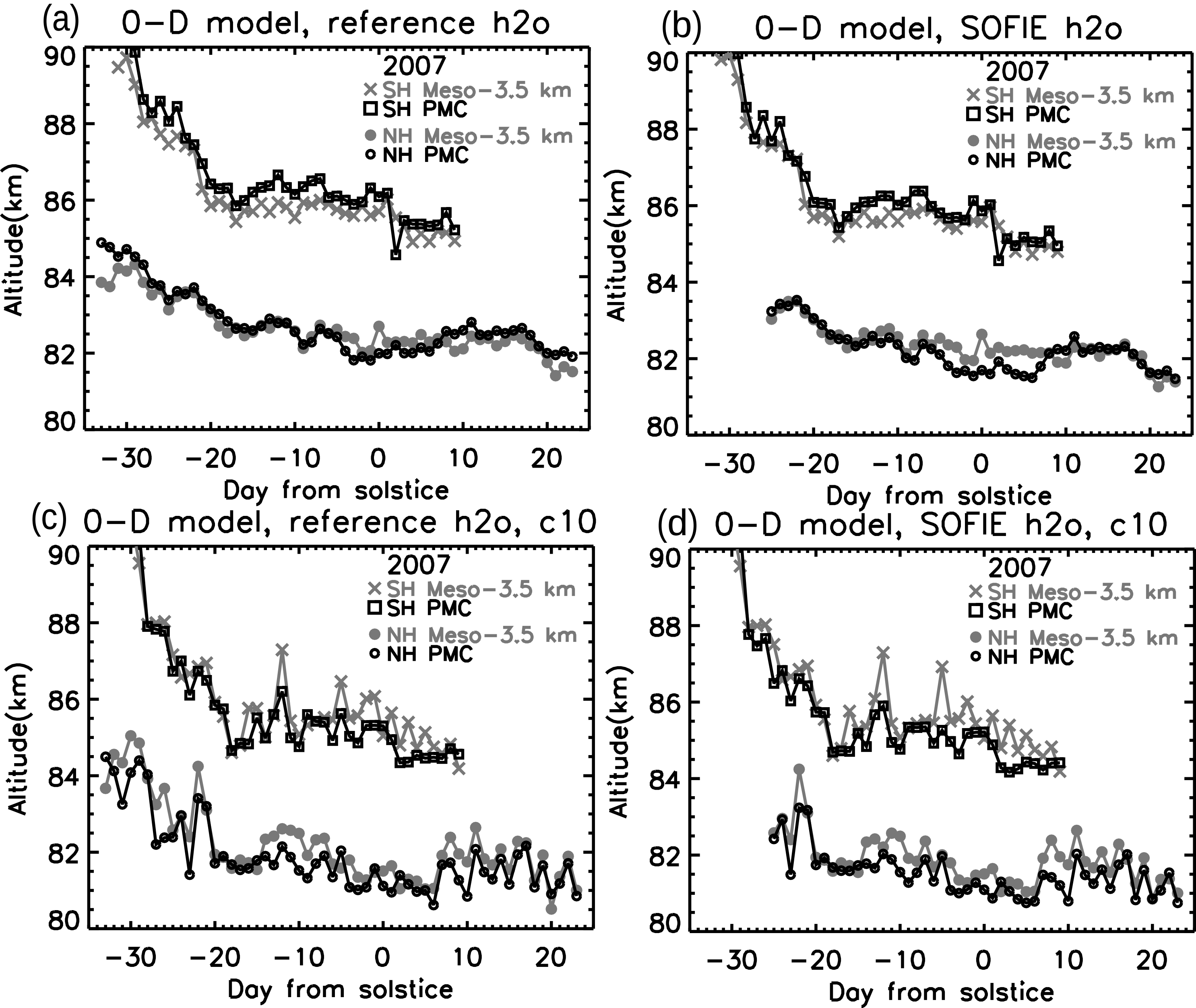

(a) 0-D model, reference h2o
(b) 0-D model, SOFIE h2o
(c) 0-D model, reference h2o, c10
(d) 0-D model, SOFIE h2o, c10
2007
SH Meso-3.5 km
SH PMC
NH Meso-3.5 km
NH PMC
Altitude(km)
Day from solstice
90
88
86
84
82
80
-30
-20
-10
0
10
20

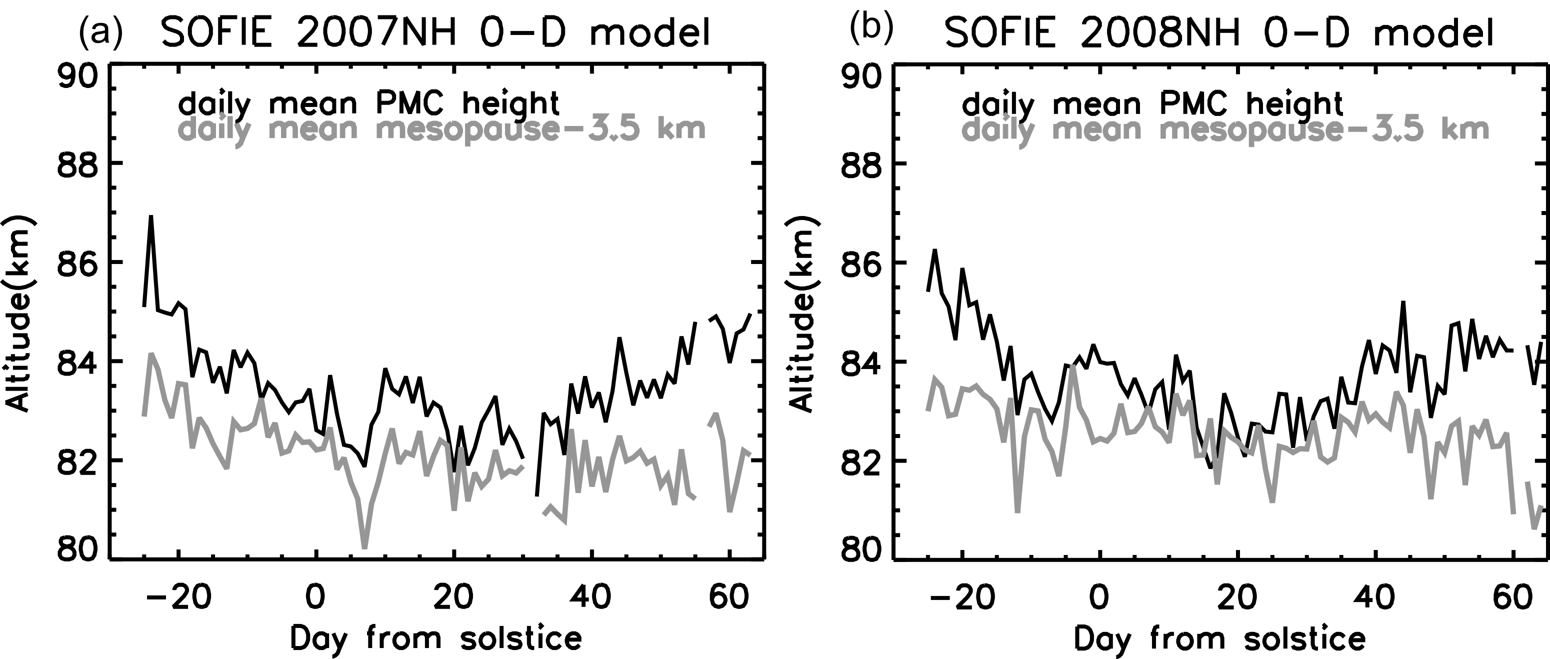
(a) SOFIE 2007NH 0-D model
daily mean PMC height
daily mean mesopause-3.5 km
Altitude(km)
90
88
86
84
82
80
-20
0
20
40
60
Day from solstice
(b) SOFIE 2008NH 0-D model
daily mean PMC height
daily mean mesopause-3.5 km
Altitude(km)
90
88
86
84
82
80
-20
0
20
40
60
Day from solstice

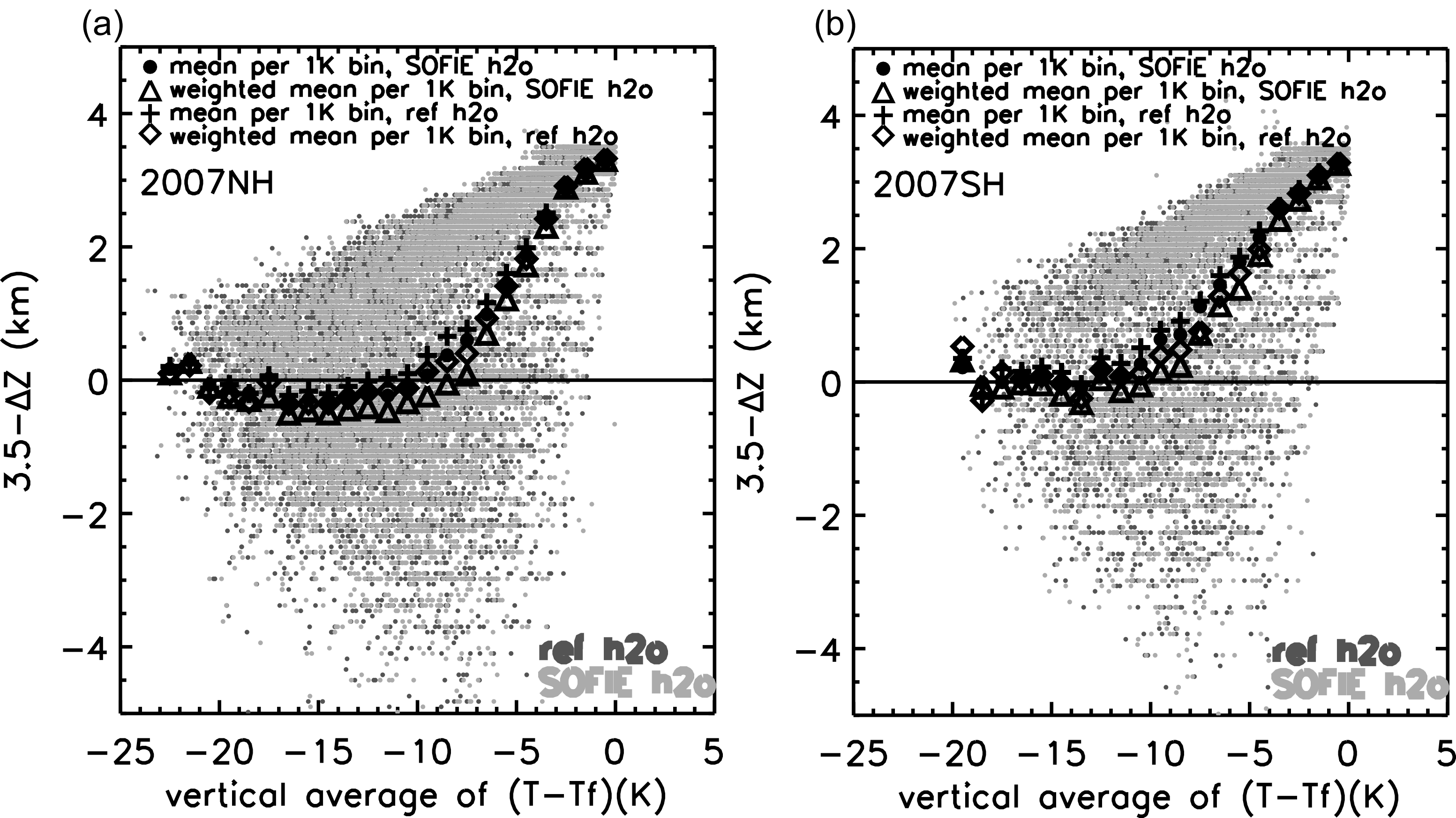

(a)
mean per 1K bin, SOFIE h2o
weighted mean per 1K bin, SOFIE h2o
mean per 1K bin, ref h2o
weighted mean per 1K bin, ref h2o
2007NH
ref h2o
SOFIE h2o
3.5−ΔZ (km)
vertical average of (T−Tf)(K)
(b)
mean per 1K bin, SOFIE h2o
weighted mean per 1K bin, SOFIE h2o
mean per 1K bin, ref h2o
weighted mean per 1K bin, ref h2o
2007SH
ref h2o
SOFIE h2o
3.5−ΔZ (km)
vertical average of (T−Tf)(K)

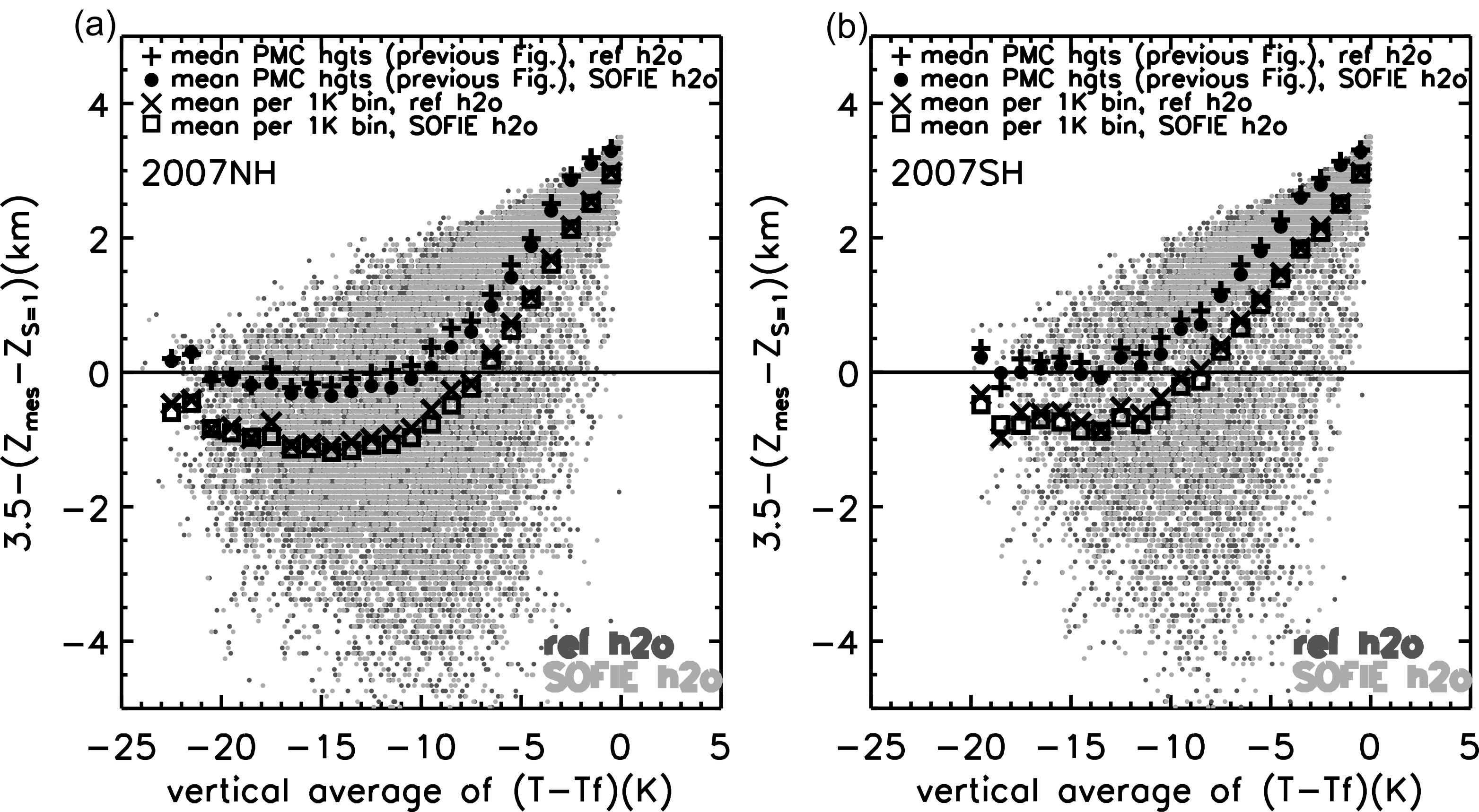

(a)
+ mean PMC hgts (previous Fig.), ref h2o
● mean PMC hgts (previous Fig.), SOFIE h2o
× mean per 1K bin, ref h2o
□ mean per 1K bin, SOFIE h2o
2007NH
ref h2o
SOFIE h2o
3.5−(Z_mes − Z_S=1)(km)
vertical average of (T−Tf)(K)
(b)
+ mean PMC hgts (previous Fig.), ref h2o
● mean PMC hgts (previous Fig.), SOFIE h2o
× mean per 1K bin, ref h2o
□ mean per 1K bin, SOFIE h2o
2007SH
ref h2o
SOFIE h2o
3.5−(Z_mes − Z_S=1)(km)
vertical average of (T−Tf)(K)

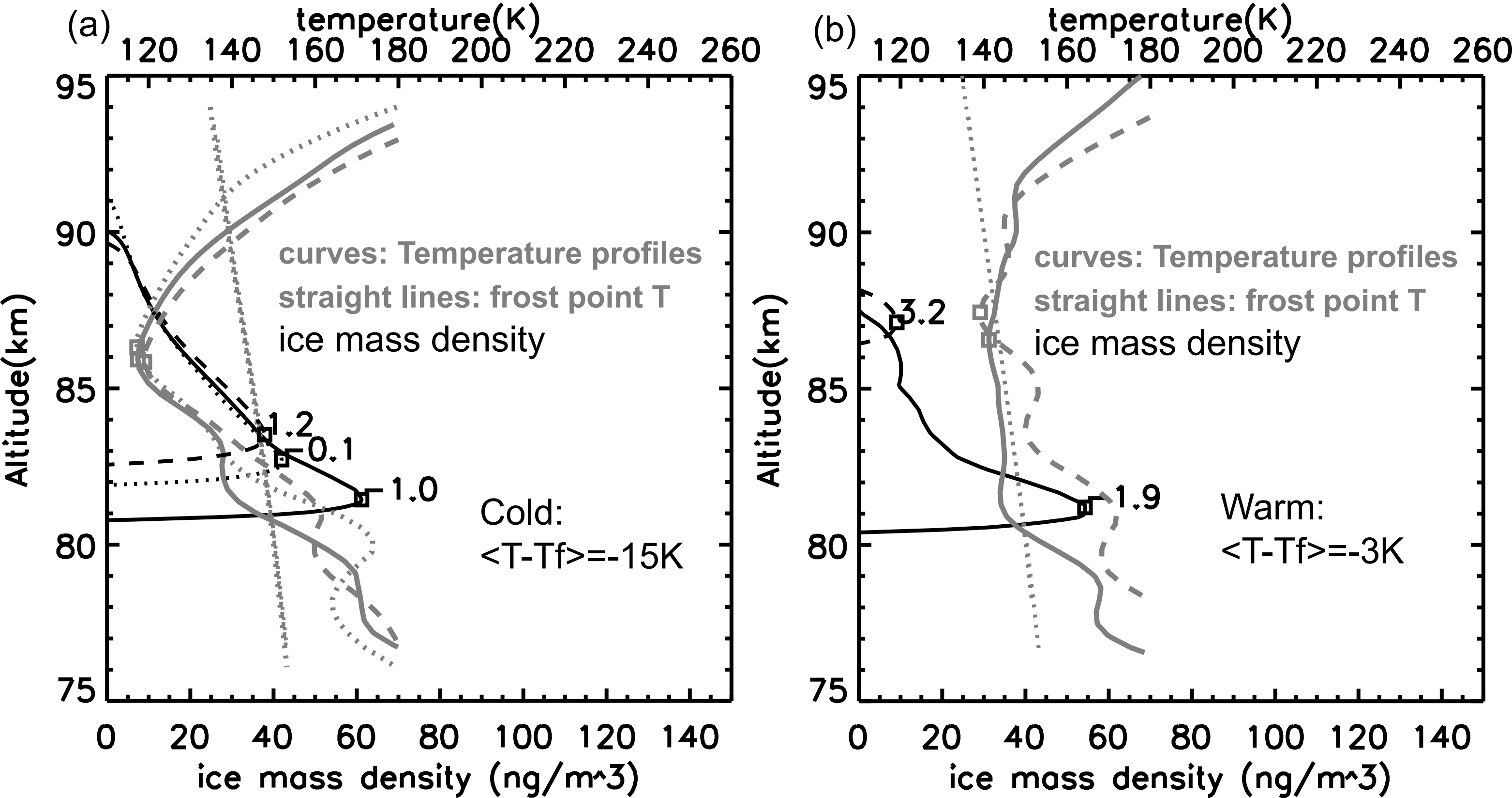

(a)
temperature(K)
120
140
160
180
200
220
240
260
95
90
85
80
75
Altitude(km)
curves: Temperature profiles
straight lines: frost point T
ice mass density
1.2
0.1
1.0
Cold:
<T-Tf>=-15K
0
20
40
60
80
100
120
140
ice mass density (ng/m^3)
(b)
temperature(K)
120
140
160
180
200
220
240
260
95
90
85
80
75
Altitude(km)
curves: Temperature profiles
straight lines: frost point T
ice mass density
3.2
1.9
Warm:
<T-Tf>=-3K
0
20
40
60
80
100
120
140
ice mass density (ng/m^3)

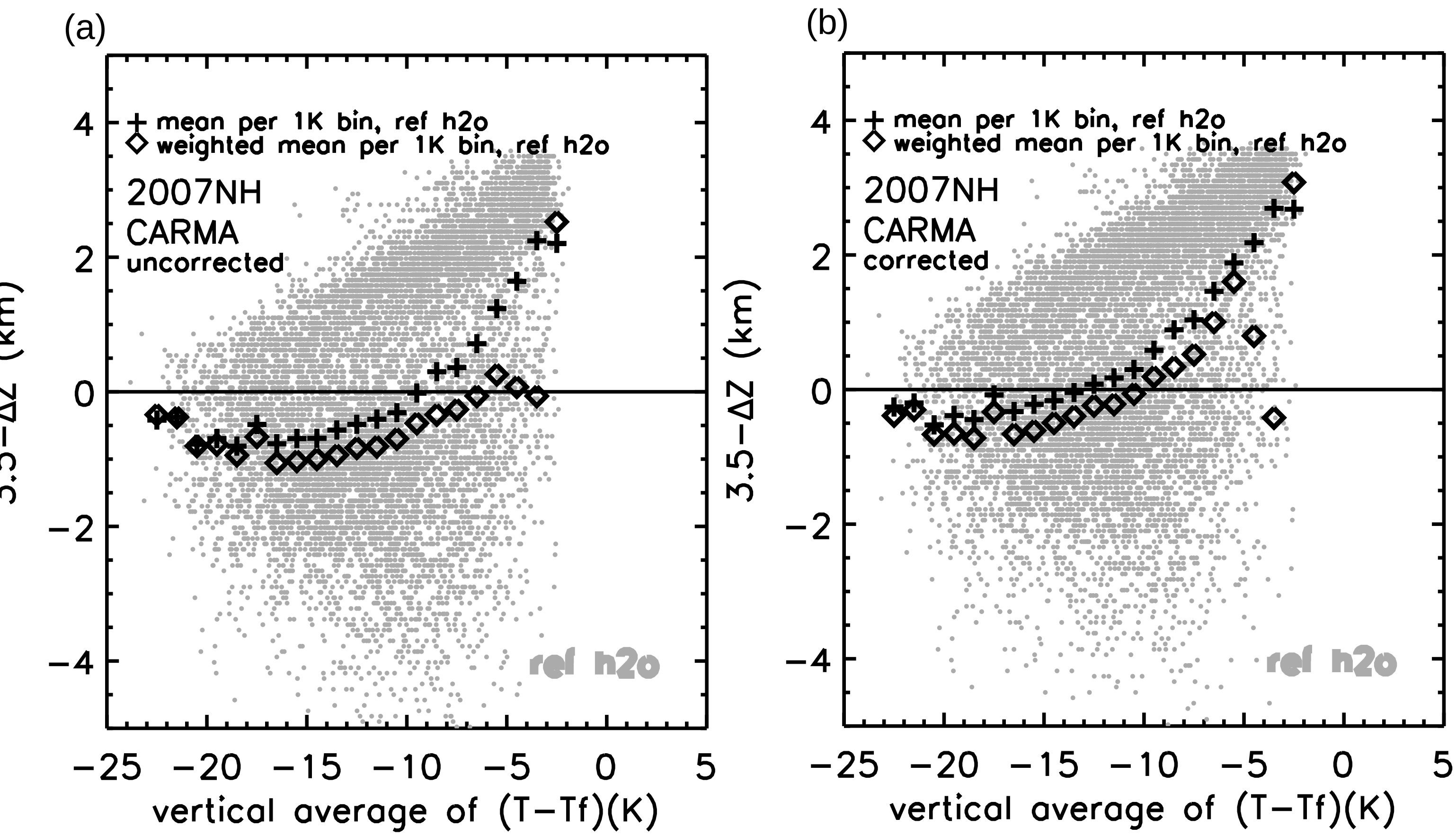

(a)
+ mean per 1K bin, ref h2o
◇ weighted mean per 1K bin, ref h2o
2007NH
CARMA
uncorrected
ref h2o
3.5−ΔZ (km)
vertical average of (T−Tf)(K)
(b)
+ mean per 1K bin, ref h2o
◇ weighted mean per 1K bin, ref h2o
2007NH
CARMA
corrected
ref h2o
3.5−ΔZ (km)
vertical average of (T−Tf)(K)

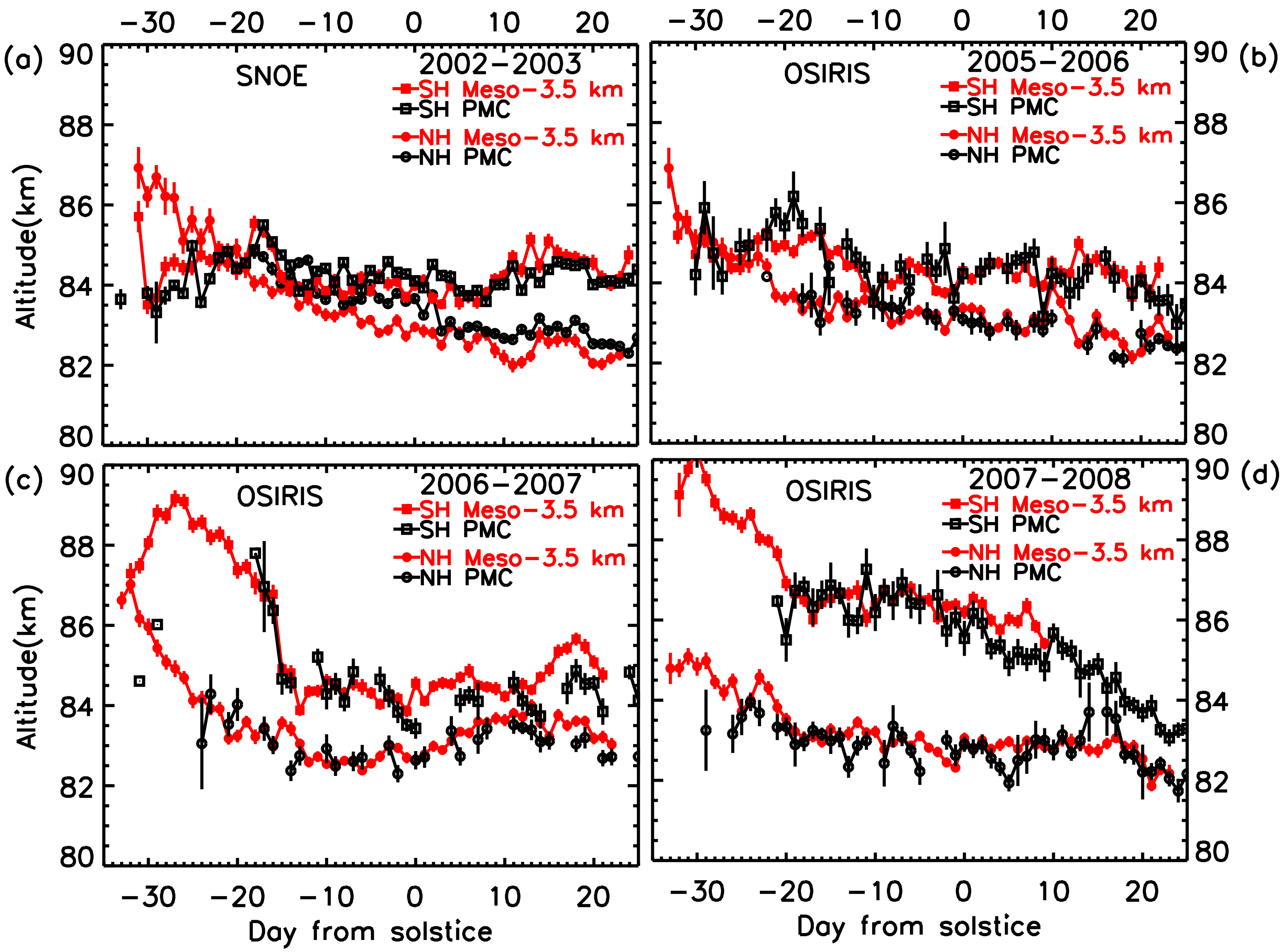
(a)
SNOE
2002−2003
SH Meso−3.5 km
SH PMC
NH Meso−3.5 km
NH PMC
(b)
OSIRIS
2005−2006
SH Meso−3.5 km
SH PMC
NH Meso−3.5 km
NH PMC
(c)
OSIRIS
2006−2007
SH Meso−3.5 km
SH PMC
NH Meso−3.5 km
NH PMC
(d)
OSIRIS
2007−2008
SH Meso−3.5 km
SH PMC
NH Meso−3.5 km
NH PMC
Altitude(km)
Day from solstice

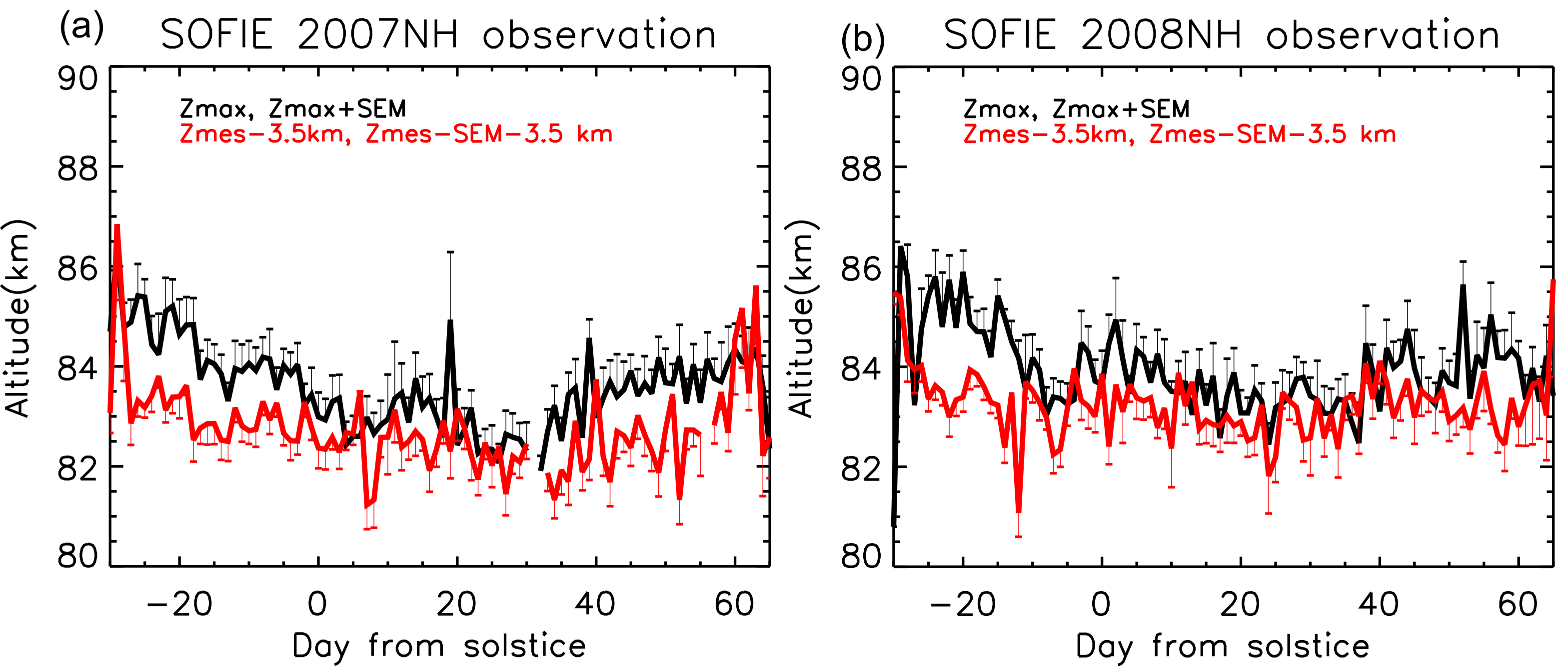
(a)
SOFIE 2007NH observation
Zmax, Zmax+SEM
Zmes−3.5km, Zmes−SEM−3.5 km
Altitude(km)
90
88
86
84
82
80
−20
0
20
40
60
Day from solstice
(b)
SOFIE 2008NH observation
Zmax, Zmax+SEM
Zmes−3.5km, Zmes−SEM−3.5 km
Altitude(km)
90
88
86
84
82
80
−20
0
20
40
60
Day from solstice

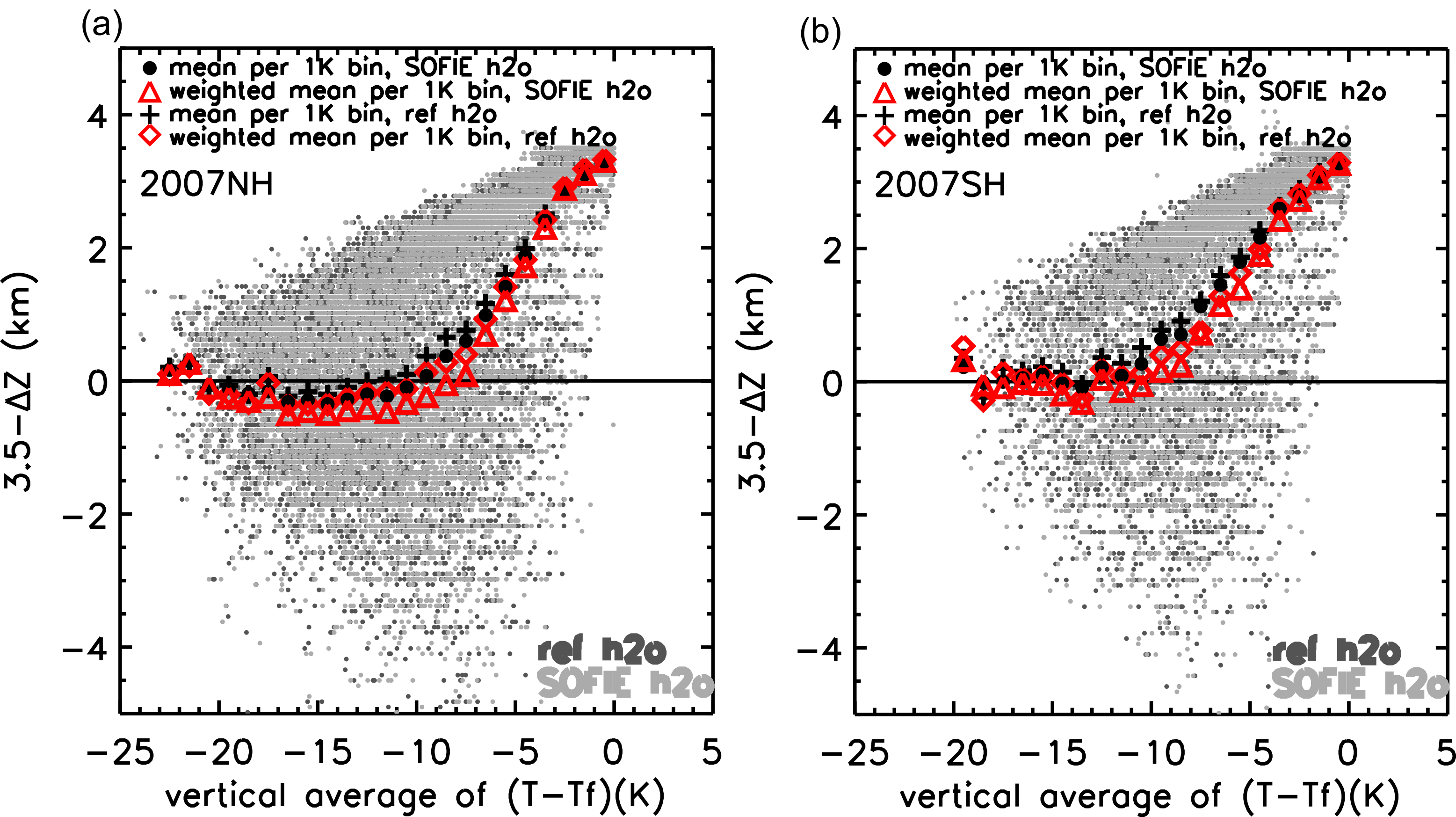

(a)
mean per 1K bin, SOFIE h2o
weighted mean per 1K bin, SOFIE h2o
mean per 1K bin, ref h2o
weighted mean per 1K bin, ref h2o
2007NH
ref h2o
SOFIE h2o
3.5−ΔZ (km)
vertical average of (T−Tf)(K)
4
2
0
−2
−4
−25
−20
−15
−10
−5
0
5
(b)
mean per 1K bin, SOFIE h2o
weighted mean per 1K bin, SOFIE h2o
mean per 1K bin, ref h2o
weighted mean per 1K bin, ref h2o
2007SH
ref h2o
SOFIE h2o
3.5−ΔZ (km)
vertical average of (T−Tf)(K)